IEEE Access
Multidisciplinary | Rapid Review | Open Access Journal

Received 3 May 2024, accepted 4 June 2024, date of publication 12 June 2024, date of current version 19 June 2024.

Digital Object Identifier 10.1109/ACCESS.2024.3413389

RESEARCH ARTICLE

Mission-Compliant Optimal Sensor Formation Positioning for Range-Based Underwater Localization

DANIELA DE PALMA, SIMONE DE NICOLI, AND GIANFRANCO PARLANGELI, (Member, IEEE)
Department of Engineering for Innovation, University of Salento, 73100 Lecce, Italy
Corresponding author: Daniela De Palma (daniela.depalma@unisalento.it)

ABSTRACT This paper proposes an optimal sensor formation strategy for range-based underwater localization of a team of vehicles. The problem is addressed by considering sensor deployment area constraints typical of realistic and complex scenarios so that a mission-compliant optimal sensor formation is derived. Communication constraints, safety requirements, maximal platform speed limitations, and physical constraints imposed by the mission are explicitly incorporated into the estimation framework. The resulting problem is formulated as an unconstrained optimization problem that allows the use of global optimization tools that can numerically construct optimal placements. The approach is also extended to a more realistic scenario, in which the positions of the targets are known with some degree of uncertainty. Extensive simulations corroborate the effectiveness of the proposed strategy for different configurations involving an arbitrary number of sensors and targets. This confirmed its potential use as a pre-planning tool for realistic and practical mission scenarios.

INDEX TERMS Optimal sensor placement, range-based localization, sensor network, target tracking.

I. INTRODUCTION

During the last few decades, there has been impressive thrust for the development of autonomous marine devices such as Unmanned Surface vessels (USVs), Autonomous Surface Vehicles (ASVs), and Autonomous Underwater Vehicles (AUVs). Motivated by their impact on an increasing number of applications, relatively low costs, and the replacement of human operators in hazardous conditions, both underwater and surface vehicles have become key elements for the exploration and exploitation of marine resources.

Typical missions include, but are not limited to, ocean exploration, bathymetric data collection, geophysical and geotechnical surveying, ocean cable inspection, earthquake prediction, and harbor patrolling. Moreover, it is becoming increasingly common to design missions by exploiting a team of autonomous underwater vehicles working cooperatively [1]. This choice allows us to reach mission goals that are not possible when using a single vehicle [2], [3].

The associate editor coordinating the review of this manuscript and approving it for publication was Wai-Keung Fung.

Regardless of the specific application, mission success is strongly based on the capability of a vehicle to localize itself and navigate with the required accuracy. In the harsh operating conditions of the underwater environment, navigation is a challenging research field because of the impossibility of relying on radio-based communications and radio-based localization (GPS - Global Positioning System).

Conventional methods for localization and navigation of AUVs rely on high-resolution (and expensive) Inertial Navigation Systems (INS) integrated with Doppler Velocity Log (DVL) sensors and/or with frequent surfacing of AUVs for GPS fix [4].

Alternative approaches make use of acoustic devices that, through the measurement of the time-of-flight of acoustic signals, allow for estimating the ranges from AUVs to receiving nodes positioned at known locations. Typical underwater acoustic positioning systems include three main categories, long baseline (LBL), short baseline (SBL), and ultra-short baseline (USBL), based on the distance between the hydrophones that receive the signals emitted by the AUV. Though effective, all these approaches have the drawback of high costs, the necessity to stop AUV

operations to go for GPS feed, or the limitation of the area of interest.

Recently, a novel approach to underwater localization has emerged: *cooperative localization* [5]. In this setup, a few autonomous (surface or underwater) vehicles, called sensors (or buoy vehicles/beacon vehicles), lie on the water surface or resurface frequently for GPS signals so that their exact positions are assumed to be known. Other underwater vehicles, called targets, accurately localize themselves by exploiting the relative range and/or bearing measurements from referenced sensors. Range and/or bearing information can be retrieved from data of different natures, such as the Received Signal Strength (RSS), Time Difference of Arrival (TDOA), Time of Arrival (TOA), or Angle of Arrival (AOA) of signals sent between targets and sensors [6], [7].

Regardless of the nature of the information, the geometry between the sensors and targets strongly affects the performance of the localization system. Indeed, on one hand, acoustic positioning systems require accurate knowledge of sensor locations, since errors in these positions induce errors in the estimation of the target positions. On the other hand, an appropriate positioning of the sensors allows accurate localization of the targets. Hence, the sensor formation plays a crucial role in the performance of such localization systems. Therefore, special attention has been devoted to the optimal positioning of the sensors to improve the accuracy of the target positioning system, and in recent years, it has become a significant research field.

In this paper, we focus on a cooperative localization system based on range-only measurements between sensors and targets. The objective is to determine the optimal geometric configuration of a sensor network that maximizes the range-related information available for underwater target positioning in real and more complex mission scenarios.

A. RELATED WORKS

Here we describe the most significant literature related to sensor placement for cooperative localization. One of the first results goes back to the work in [8], where the authors addressed the problem of finding sensor arrangements to estimate a source position more accurately from the received sensor signals. A simple method, based on the minimization of the Cramer-Rao lower bound (CRLB) variance, was developed for optimally placing sensors subject to the constraint of aligned sensors.

An interesting methodological study in the area of optimal sensor placement for ground robots has been presented by Martinez and Bullo in [9]. The work focused on optimal sensor placement for mobile sensor networks in single target-tracking applications. They show that in an optimal configuration, the sensors are uniformly placed in a circular fashion around the target, and propose a motion coordination strategy to steer the mobile sensor network to the optimal deployment. This result for range-based localization was also analytically demonstrated in [10]. The authors show that for a number of sensors greater than three, the best solution is obtained by arranging the sensors uniformly with respect to the target, that is, with neighboring sensors separated by equal angle increments. If the number of sensors is two, the optimal sensor-target geometry is unique and occurs when the angle subtended at the target is equal to ninety degrees. The optimal sensor-target geometries for time-of-arrival-based and bearing-only localization are also identified and studied in this work.

More recently, the problem of optimal sensor positioning for cooperative range-based localization has been explicitly addressed in underwater environments. A milestone contribution is represented by the works in [11], [12], and [13] by Moreno-Salinas et al.

In [11] the problem of optimal sensor placement for multiple target positioning with range-only measurements in an unconstrained 2-D scenario is studied. First, the authors addressed the problem of single-target positioning. They derived the same optimal solutions for sensor placement given in the above-mentioned references [9], [10] using a different methodology. They also defined, in a rigorous manner, the optimality conditions that the sensor formation must satisfy to minimize the error in the estimation of the target position. The problem is then extended to a multiple-target positioning scenario. The two-target positioning problem is solved analytically and numerically, using the tools of estimation theory, by minimizing a properly defined object function based on the Fisher Information Matrices associated with each of the targets. The problem of localizing an arbitrary number of targets is complex and cannot always be solved analytically. For the cases where the objective function exhibits convexity in the search domain, convex optimization tools are used to determine the optimal sensor configurations.

In [12] the problem of single-target positioning is addressed in a 3-D scenario. The special case of an underwater target localized by an (ocean) surface sensor network is studied, leading to a 3-D scenario where the sensor array is placed on a plane (2-D). A solution is also provided for the particular case in which the target depth is known, avoiding the need to estimate it through the sensor array. In [13] the analysis of the 3-D scenario is extended to the multi-target positioning case. It is shown that for a scenario with three sensors and two targets, the objective function based on the Fisher Information Matrices is convex, and thus, it is possible to define an optimal sensor configuration that yields high positioning accuracy for both targets simultaneously, using convex optimization tools. However, if the problem becomes too complex, for example, for more than two targets and three sensors, it is no longer possible to prove the convexity of the objective function in the domain space. Moreover, it may be necessary to trade-off the localization accuracy of each target. As a result, non-convex optimization techniques are required. The authors present a potential solution based on a global numerical optimization procedure known as ''Simulated Annealing''.

Given the relevance and challenging issues related to the optimal sensor formation for cooperative localization of

AUVs, in 2019, a review article [5] presented a comparative survey of existing techniques. This work may be a reference material for those who wish to deepen the topic at hand. The main challenges identified in this review are related to the fact that, in real applications, sensors cannot be placed anywhere, but the sensor deployment area is subject to constraints such as geographic limitations, communication problems between sensor pairs, and safety concerns. Moreover, the range measurements between sensors and targets are acquired using acoustic devices; therefore, they are affected by measurement noise, which depends on multiple factors. In realistic scenarios, it is (at least) distance-dependent. Nevertheless, there are only a few works that consider a distance-dependent measurement noise, most of the research, for example, [9], [11] still assume a zero mean Gaussian noise with constant covariance. Furthermore, computational effort is another crucial issue. Indeed, in the complex scenario of multi-target positioning, the optimal sensor formation must be computed simultaneously for all targets, leading to an increase in computational complexity and time.

Finally, one of the most important challenges is that none of the proposed methods have been experimentally validated in a real environment. Thus, there is a strong need for experimental verification to improve the methodological methods by addressing the shortcomings that emerge during experiments. Actually, the most recent research activities [14], [15], [16], [17] are moving in these directions. The work in [14] deals with the problem of optimal positioning of sensors on the sea surface for the localization of multiple underwater targets that operate at a constant and known depth; thus, it is similar to that addressed in [13]. The major difference with respect to [13] is related to the characteristics of the measurement noise, which is assumed to be distance-dependent rather than zero-mean Gaussian noise with constant covariance. Given the complexity of the scenario, the problem is solved using a numerical global optimization algorithm based on the annealing idea.

In [15], the authors consider the problem of optimal sensor positioning under deployment area constraints. First, they analyzed the case in which there are two sensors that can only be arranged within a circular area. Then, the results are extended to a larger number of sensors in a region of arbitrary shape.

Also in the work [16], the authors consider the problem of optimal sensor placement (based on the time difference of the arrival measurement) with some communication constraints. They assumed that sensors can communicate with a reference sensor only when the distance between the sensor and reference is less than a given constant value. They theoretically analyze the optimal sensor-source (target) geometry with an arbitrary number of sensors in two cases: when the source (target) is inside and outside the sensor placement area.

The paper [17] analyzes the optimal positioning of sensors for the simultaneous localization of two targets on the two-dimensional plane exploiting time-of-arrival (TOA) measurements. The scenario under investigation has a total of $n + 2m$ sensors, where each target has m sensors associated with only that target, while n sensors, or shared sensors, collect data from both targets. Performances are evaluated through the CRLB trace. The authors [17] show that optimal sensor placement can occur when the shared sensors are located in the midline between the two targets.

Some communication and safety constraints are considered in [18] for a similar single-target localization problem based on the Angle Of Arrival. The considered scenario takes into account two constraints: 1) the sensors and the target placed within a circular constrained region; 2) the relative distance between the sensors and the target is greater than the minimum safe distance. The optimal sensor formation problem is tackled as a constrained optimization problem. To make it mathematically solvable and to reduce its complexity, equivalent and easier constraints are established using the introduced maximum feasible angle and optimal separation angle. The solution is analyzed explicitly for only two and three sensors. However, as the number of sensors increases, the problem becomes analytically complex and difficult to be solved.

The work in [19] represents the first contribution that considers a relatively complex scenario by employing a range-dependent model of measurement noise and by taking into account the performance metrics (to evaluate the localization performance) of the entire planned trajectory of the target. Indeed, the authors explicitly addressed the problem of optimum sensor placement in a plane for the localization of an underwater vehicle moving in 3D along a preplanned trajectory. To solve the problem a genetic algorithm is employed to maximize a proper objective function. This objective function is based on the arithmetic mean along the vehicle's trajectory of the largest eigenvalue of the inverse of the Fisher information matrix. In addition, a multi-objective problem is considered, in which pairs of metrics based on the Fisher information matrix are analyzed.

At this point, it is worth highlighting that while there is a quite extensive literature on the subject, there is still work to be done to bridge such theoretical approaches and recommendations with practical implementation for real-world applications. Indeed, there has not been any experimental verification of any of the proposed methods yet. Integrating mission-specific considerations into the formulation of the problem represents a step towards facilitating experimental verification of proposed methods. The existing methods do not take simultaneously into account mission-specific considerations such as the limit on the maximal feasible velocity of the vehicles along the planned trajectory, the limits on the safety distance between vehicles, or the measuring distance. Such aspects represent a key point that makes the problem more complex and are essential for experimental verification.

B. SCOPE AND CONTRIBUTIONS

Motivated by the challenging issues raised in this field, the present work addresses the problem of optimal sensor

formation by considering several constraints involved in real multiple-vehicle scenarios of practical interest.

The contributions are twofold:

i) We modified the existing methods by explicitly integrating mission constraints in the problem formulation. Mission-related considerations such as vehicles maximal velocity constraints, safety constraints, or the measuring distance, make the problem complex when the constraints are considered simultaneously, especially when the number of vehicles (sensors and targets) increases. Our main contribution is on adapting the existing optimal sensor placement solutions to practical scenarios in real-world applications with the aim of facilitating an experimental validation of proposed methods.

ii) Our ultimate contribution aims at incorporating these mission constraints into the general optimal sensor formation problem in a simple way, leaving the problem (numerically) tractable and maintaining the ability to compute solutions efficiently. Indeed, the resulting constrained optimization problem is recast into an unconstrained optimization problem, simplifying the structure and allowing the use of global optimization tools for the solution.

The above framework represents a challenging and essential scenario for direct experimental verification. This analysis represents a preliminary step towards experimental validations of optimal sensor formation algorithms for range-based underwater localization of AUVs in a realistic and complex mission environment.

C. ORGANIZATION OF THE ARTICLE

The rest of the paper is organized as follows. Section II presents the sensor formation problem and the addressed scenario (common to most marine missions). In Section III, the optimal sensor formation problem is formulated and the FIM for a generic network with n sensors and m targets is presented in the assumptions under investigation. Section IV is dedicated to the modeling of the considered constraints imposed by the mission. The objective function to be maximized to solve the optimal sensor formation problem under the considered constraints is presented in Section V. The numerical solution of this optimization problem is discussed in Section VI. Section VII describes and analyzes the numerical simulations of the proposed algorithm. The more realistic scenario where the positions of the targets are known with some uncertainty is addressed in Section VIII. Finally, concluding remarks are summarized in Section IX.

II. MOTIVATING SCENARIO

The problem at hand is addressed with the goal of offering a solution that may be used as a pre-planning tool in realistic and practical mission scenarios.

Consider an arbitrary number of sensors, referenced *"buoys vehicles"* in the following, namely vehicles placed on the sea surface that have access to a georeferenced system,

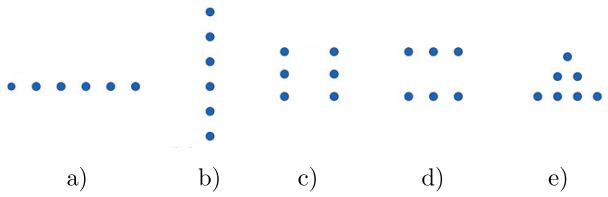

FIGURE 1. Types of formation: a) "alongside", b) "single line", c) "double line", d) "double alongside" and e) "triangular".

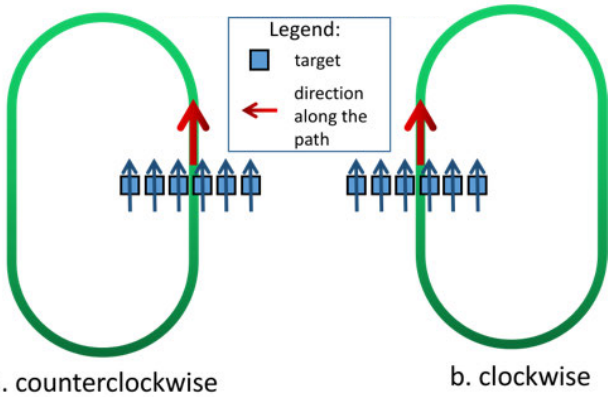

FIGURE 2. Counterclockwise and clockwise directions along a racecourse path with targets in alongside formation.

and an arbitrary number of targets, namely autonomous underwater vehicles typically operating at a certain depth in formation and occasionally resurfacing for mission purposes.

For example, common formations of practical interest are *"alongside"*, *"single line"*, *"double alongside"*, *"double line"* and *"triangular"*(as illustrated in Fig. 1).

We assume that the target vehicles move in formation following preassigned paths, such as circular path, or racecourse path, with a specific direction, i.e. counterclockwise or clockwise (see for example figure 2) as in most marine applications.

Indeed, we are interested in finding the optimal feasible position of the sensors with respect to the specific formation of the targets so that, if all vehicles, sensors and targets, maintain the formation, the localization system achieves the best performance (figure 3).

In realistic applications, sensors cannot be placed anywhere over the area of interest. The feasible sensor deployment is subjected to restrictions due to communication or measuring constraints, safety requirements, maximal platform speed limitation, or physical constraints imposed by the mission. Hence, the optimal positioning of the sensors must be carried out considering a proper constraints set.

A minimum distance for safety must be maintained between the vehicles to avoid accidents or possible collisions. Even if the vehicles are immersed in the sea, they may need to rise to the surface and, if there is no minimum distance between targets and sensors, a collision can occur.

In addition, sensors cannot be positioned too far from the target vehicles because range measurements are effective only within a certain distance in the water.

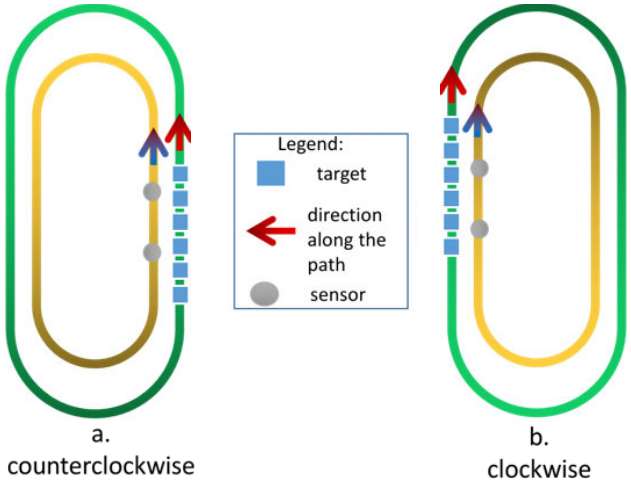

FIGURE 3. Example of optimal sensors configuration with targets moving in single line formation along a racecourse path.

Finally, during the mission both the targets and the sensors are in motion. Hence, it is important to verify that the formation during the mission is compatible with the physical limits of the vehicles (sensors and targets), i.e. with their maximum speeds.

III. PROBLEM FORMULATION

In this Section, we state the optimal sensor placement problem for range-based multiple target positioning in a 3D scenario. Consider an inertial reference system $\{I\}$ with axes $\{x_I\}$, $\{y_I\}$ and $\{z_I\}$, and the general case with m targets and n sensors. Consider a Cartesian coordinate space centered in the center C_m of the nominal target formation and with $x-y$ axes along the horizontal and vertical direction of the formation. We denote this moving local reference frame as $\{\mathcal{O}\}$ in the following. The depth of the target vehicles is assumed to be known; indeed, in many practical applications, the target depth can be measured directly with a depth sensor, usually characterized by small error and low cost; we also assume that the sensors at the surface have access to this information.

The position for the $j-th$ target in $\{\mathcal{O}\}$ is denoted by $q_j = [q_{jx}, q_{jy}, q_{jz}]$ with $j = 1, 2, \ldots, m$ and the position for the $i-th$ sensor in $\{\mathcal{O}\}$ is denoted by $p_i = [p_{ix}, p_{iy}, p_{iz}]$ with $i = 1, 2, \ldots, n$. Denote by $q \in \mathbb{R}^{m\times 3}$ the matrix of targets positions and by $p \in \mathbb{R}^{n\times 3}$ the matrix of sensors positions as follows:

$$q = \begin{bmatrix} q_{1x} & q_{1y} & q_{1z} \\ q_{2x} & q_{2y} & q_{2z} \\ \cdots & \cdots & \cdots \\ q_{mx} & q_{my} & q_{mz} \end{bmatrix} \tag{1}$$

$$p = \begin{bmatrix} p_{1x} & p_{1y} & p_{1z} \\ p_{2x} & p_{2y} & p_{2z} \\ \cdots & \cdots & \cdots \\ p_{nx} & p_{ny} & p_{nz} \end{bmatrix}. \tag{2}$$

An example of the scenario under investigation is sketched in figure 4.

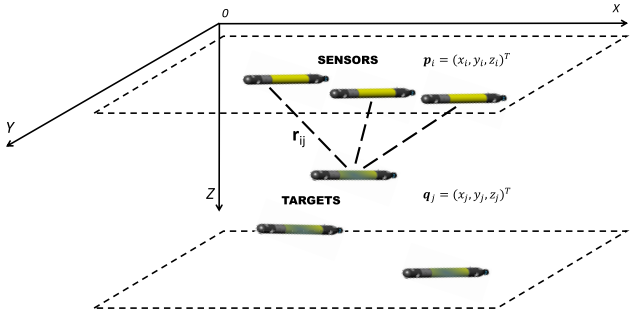

FIGURE 4. Multi-targets cooperative localization model in 3D with m=3 targets and n=3 sensors.

Let r_{ij} denote the euclidean distance between the $i-th$ sensor and the $j-th$ target, namely:

$$r_{ij} = \sqrt{(p_{ix} - q_{jx})^2 + (p_{iy} - q_{jy})^2 + (p_{iz} - q_{jz})^2}, \tag{3}$$

and the related distance matrix $r \in \mathbb{R}^{n\times m}$ defined as:

$$r = \begin{bmatrix} r_{11} & r_{12} & r_{13} & \ldots & r_{1m} \\ r_{21} & r_{22} & r_{23} & \ldots & r_{2m} \\ \cdots & \cdots & \cdots & \cdots & \cdots \\ r_{n1} & r_{n2} & r_{n3} & \ldots & r_{nm} \end{bmatrix}. \tag{4}$$

In the following, vector r_j denotes the vector of the actual distance between the $j-th$ target and each of the n sensors (Eq. 4):

$$r_j = \begin{bmatrix} r_{1j} \\ r_{2j} \\ \cdots \\ r_{nj} \end{bmatrix} \text{ with } j = 1, 2, \ldots, m. \tag{5}$$

We assume that range measurements r_{ij} are affected by additive noise w_{ij}. The measurement error vector $w_j = [w_{1j}, w_{2j}, \ldots, w_{nj}]^T$ $j = 1, 2, \ldots, m$ is made by the $j-th$ target and all sensors. All noise sources are assumed to be independent and are zero mean Gaussian processes, $N(0_n, \Sigma)$, with $\Sigma = diag(\sigma_1, \ldots, \sigma_n)$. For the sake of simplicity, all sensors are assumed to have the same variance $\sigma_i^2 = \sigma^2$ for $i = 1, 2, \ldots, n$, so that $\Sigma = \sigma^2 \cdot I_n$. The measure captured by the $i-th$ sensor from the $j-th$ target is:

$$z_{ij} = r_{ij} + w_{ij} \tag{6}$$

with $i = 1, 2, \ldots, n$ and $j = 1, 2, \ldots, m$. Therefore, we define the matrix of measurements $z \in \mathbb{R}^{n\times m}$

$$z = \begin{bmatrix} z_{11} & z_{12} & z_{13} & \ldots & z_{1m} \\ z_{21} & z_{22} & z_{23} & \ldots & z_{2m} \\ \cdots & \cdots & \cdots & \cdots & \cdots \\ z_{n1} & z_{n2} & z_{n3} & \ldots & z_{nm} \end{bmatrix}. \tag{7}$$

The cooperative localization measurement equation for the $j-th$ target is given as follows:

$$z_j = \begin{bmatrix} z_{1j} \\ z_{2j} \\ \cdots \\ z_{nj} \end{bmatrix} \sim N(r_j, \Sigma) \text{ with } j = 1, 2, \ldots, m. \tag{8}$$

Since the noise is assumed to be a Gaussian random variable, also the measurement is assumed to be a Gaussian random variable with mean r_j and variance Σ.

Following what is commonly reported in the literatures [9] and [20], the optimal sensor formation is evaluated by examining the so-called Fisher Information Matrix (FIM). The FIM provides a measure of the amount of information provided by the measurements about an estimation process [21]. The FIM related to the problem of range-based positioning of the target q_j can be computed from the likelihood function $L(q_j)$ given by:

$$L(q_j) = \frac{1}{(2\pi)^{\frac{n}{2}}|\Sigma|^{\frac{1}{2}}} e^{-\frac{1}{2}(z_j - r_j)^T \Sigma^{-1}(z_j - r_j)}, \tag{9}$$

so that, as shown in [13], the Fisher's information matrix of the $j-th$ target results in:

$$FIM(q_j) = \frac{1}{\sigma^2} \cdot \sum_{i=1}^{n} \begin{bmatrix} \frac{(p_{ix}-q_{jx})^2}{r_{ij}^2} & \frac{(p_{ix}-q_{jx})(p_{iy}-q_{jy})}{r_{ij}^2} \\ \frac{(p_{ix}-q_{jx})(p_{iy}-q_{jy})}{r_{ij}^2} & \frac{(p_{iy}-q_{jy})^2}{r_{ij}^2} \end{bmatrix}, \tag{10}$$

where the depth q_{jz} of the target vehicles is assumed to be known for $j = 1, \ldots, m$, and the plane containing the sensors is with the sea surface, thus:

$$p_{iz} = 0 \text{ for } i = 1, \ldots, n.$$

For ease of presentation, we denote the contribution associated with the $i-th$ sensor and the $j-th$ target as:

$$FIM_{ij} = \begin{bmatrix} \frac{(p_{ix}-q_{jx})^2}{r_{ij}^2} & \frac{(p_{ix}-q_{jx})(p_{iy}-q_{jy})}{r_{ij}^2} \\ \frac{(p_{ix}-q_{jx})(p_{iy}-q_{jy})}{r_{ij}^2} & \frac{(p_{iy}-q_{jy})^2}{r_{ij}^2} \end{bmatrix}, \tag{11}$$

so, eq. (10) can be rewritten in compact form as:

$$FIM(q_j) = \frac{1}{\sigma^2} \cdot \sum_{i=1}^{n} FIM_{ij}. \tag{12}$$

The determinant of the FIM can be used as an indicator of the performance that is achievable with a given sensor formation, known as ''D-optimality'' criterion. It varies inversely with the volume of the uncertainty ellipsoid for the target estimate, so we are interested in maximizing the FIM determinant. Most of the previous research in the literatures [11], [13], and [14] addresses this optimal sensor placement problem by maximizing (by proper choice of the sensor positions) a combination of the logarithms of the determinants of the Fisher Information Matrices corresponding to each of the targets, namely $FIM(q_j)$ in eq. (12). Therefore, the ''*objective function*'' $\mathcal{F}$ to be maximized is defined as:

$$\mathcal{F} = \sum_{j=1}^{m} \ln(|FIM(q_j)|) \tag{13}$$

IV. CONSTRAINTS SETUP

In real application, the sensors area is subjected to restrictions due to several constraints imposed by the mission. The most common and often unavoidable constraints can be grouped in:

- ''*communication or measuring constraints*'': they are determined by the sensors' maximum sensing range. Each sensor is characterized by a maximum distance d_{max} in which it is able to capture the acoustic signal from a target. This constraint corresponds to the distance that enables communication between vehicles, and consequently allows to retrieve range measurements from the exchanged acoustic signals.
- ''*safety distance*'': a minimum safety distance d_{min} should be maintained between targets and sensors to prevent collisions or accidents;
- ''*maximal speed limitation*'': the motion of the target/sensor in formation along the assigned path should not require a speed larger than the maximal vehicles limit. The value of this limit depends also on the type of targets' formation, the direction of travel and the radius of curvature of the specific path (circular/racecourse) to follow.

Summarizing, we consider the following constraints set:

$$\begin{cases} r_{ij} \leq d_{max} \\ r_{ij} \geq d_{min} \end{cases} \quad \begin{cases} v_i \leq v_{s_{max}} \\ v_j \leq v_{v_{max}} \end{cases}, \tag{14}$$

being v_i and v_j the speed of the sensors and targets vehicles.

The search for the optimal formation of the sensors is carried out under these constraints. Thus, the resulting problem is a constrained optimization problem that aims at maximizing the determinant of the FIM of each target within the above constraints. This optimization problem is not convex due to the non-convexity of the determinant of the FIM for an arbitrary number of sensors and targets and the non-convexity of the constraints set. Therefore finding the global maximum is a challenging task.

Note that global optimizers, such as, simulated annealing or genetic algorithms, are mostly suited to unconstrained optimization problems. In order to fit our problem into the framework of global optimizers, we recast the problem into an unconstrained optimization problem, where all constraints are incorporated into a properly shaped objective function.

The proposed strategy consists of introducing one term for each constraint into the FIM_{ij} expression in Eq. (11) that, in the case of constraint violation, cancels that sensor/target contribution. In the following, we treat each constraint separetely.

A. COMMUNICATION OR MEASURING CONSTRAINT

The constraint related to the communication or measuring condition implies that the distance r_{ij} between a sensor and a target must not exceed the maximum distance d_{max} which

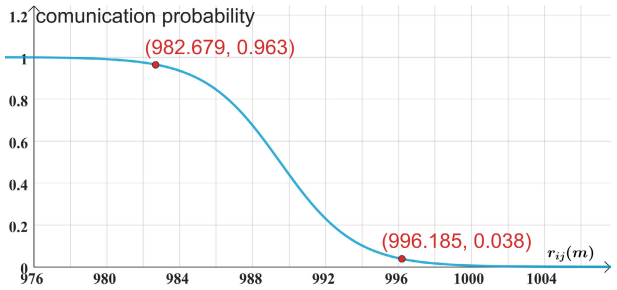

FIGURE 5. Example of sigmoid term $s_{d_{max}}(r_{ij})$ associated to the communication/measuring constraint for $d_{max} = 1000$ m.

is assumed to be constant and known a priori, namely:

$$r_{ij} \leq d_{max}. \tag{15}$$

This constraint is managed by adding a sigmoid-shaped multiplicative term $s_{d_{max}}(r_{ij})$ in the FIM in Eq.(12):

$$FIM_c(q_j) = \frac{1}{\sigma^2} \sum_{i=1}^{n} s_{d_{max}}(r_{ij}) FIM_{ij}. \tag{16}$$

The rationale behind this term $s_{d_{max}}(r_{ij})$ is to neglect the contribution to the FIM of each pair sensor/target if the relative distance r_{ij} exceeds a maximum threshold d_{max}. Indeed, if $r_{ij} > d_{max}$ the corresponding FIM contribution vanishes due to the impossibility to acquire the range measurement.

The sigmoid function is a continuous, monotonically increasing function with a characteristic 'S'-like curve, and possesses several interesting properties that make it a suitable choice in several contexts, e.g. the 'activation function' for nodes in artificial neural networks [22]. An interesting feature is that it is differentiable (a required feature in optimization algorithms), and its derivative is simple and easy to compute.

The sigmoid term introduced in the FIM to incorporate the constraint has the following expression:

$$s_{d_{max}}(r_{ij}) = \frac{1}{1 + e^{a(r_{ij} - b)}}, \tag{17}$$

with $i = 1, 2, \ldots, n$ and $j = 1, 2, \ldots, m$, where parameters $a, b \in \mathbb{R}^+$ are function of the value d_{max} and determine the steepness, starting and ending point of the 'S'-like curve. Its output has a smooth transition from values just below 1 to values above 0. In Figure 5 there is an example of sigmoid term for $d_{max} = 1000$ m. It shows how the output of the sigmoid function, that in this specific case represents the sensor/target communication probability, decreases as r_{ij} increases. In the example, it is assumed that a sensor is able to capture the acoustic signal within a distance of 1000 m, and that the decrease of the sigmoid function begins at $r_{ij} = 980$ m, and reaches the null value at $r_{ij} = 999$ m. So, it is assumed that when $r_{ij} = 980$ m, the communication probability is 0.99 while, when $r_{ij} = 999$ m, the probability of communication is 0.01. The corresponding parameters a and b are: $b = 989.5$, $a = 0.484$.

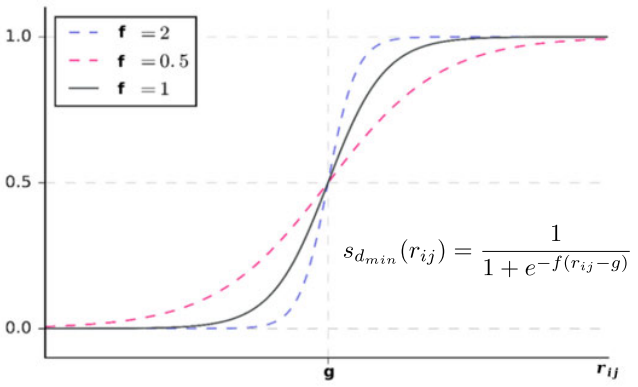

FIGURE 6. Sigmoid term $s_{d_{min}}(r_{ij})$ associated to the safety constraint.

B. SAFETY CONSTRAINT

The safety constraint requires that the distance between a sensor and a target must be larger than a given value d_{min} to prevent any collision:

$$r_{ij} \geq d_{min}. \tag{18}$$

Also in this case, this constraint is managed by inserting a multiplicative term $s_{d_{min}}(r_{ij})$ in the FIM in eq. (12) based on a sigmoid function:

$$FIM_{c'}(q_j) = \frac{1}{\sigma^2} \sum_{i=1}^{n} s_{d_{min}}(r_{ij}) FIM_{ij} \tag{19}$$

The sigmoid term introduced in the FIM to incorporate the constraint has the following expression:

$$s_{d_{min}}(r_{ij}) = \frac{1}{1 + e^{-f(r_{ij} - g)}} \tag{20}$$

with $i = 1, 2, \ldots, n$ and $j = 1, 2, \ldots, m$, where parameters $f, g \in \mathbb{R}^+$ are function of the value d_{min} and determine the steepness, starting and ending point of the transition from values near to 0 to those near to 1. Fig. 6 shows the graph of the sigmoid function $s_{d_{min}}(r_{ij})$ for different values of the parameter f.

C. MAXIMAL SPEED CONSTRAINT

The last class of constraint is related to the maximal speed limitation of the vehicles. It is instrumental to keep the vehicles speed within their maximum limit along the pre-planned path. To this effect, it is worth noting that, as highlighted in Section II, the sensors and target vehicles are assumed to travel in formation along pre-planned circular or racecourse paths with a specific direction (clockwise or counterclockwise). Fig. 7 shows a view from the top of a scenario with $m = 4$ vehicles in horizontal formation moving along a racecourse path with a counterclockwise direction. Each target follows a circular path with center at C_c in a plane parallel to the sea surface but at a given depth d_z. The sensor formation follows analogous paths in the plane $z = 0$ with center at C_c'. Let C_m be the center of the target formation, and let R_c be its radius of curvature in the circular sections.

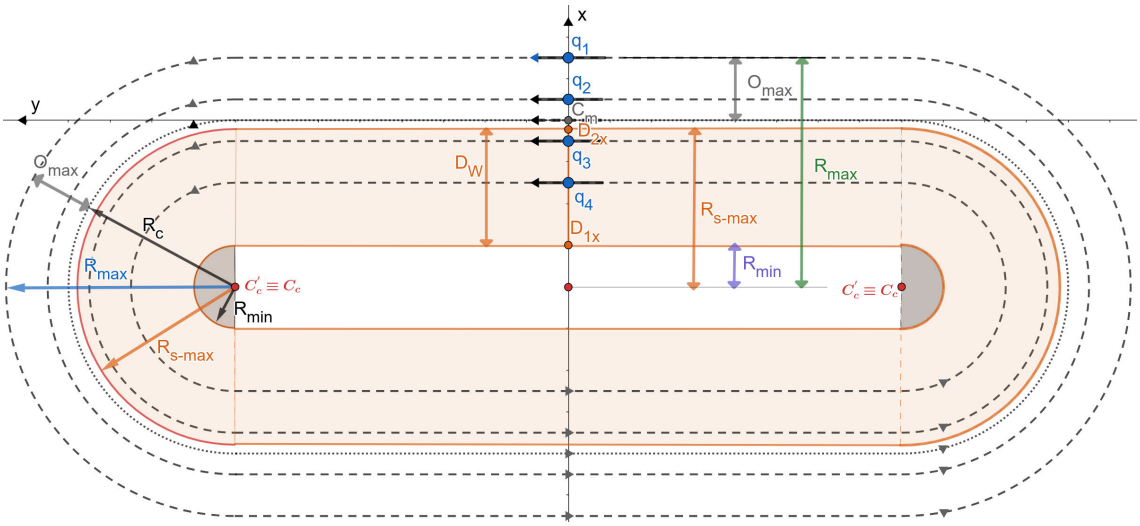

FIGURE 7. Sketch of $m = 4$ vehicles in horizontal formation moving along a racecourse path with a counterclockwise direction. Feasible sensor deployment area along the path is highlighted in orange.

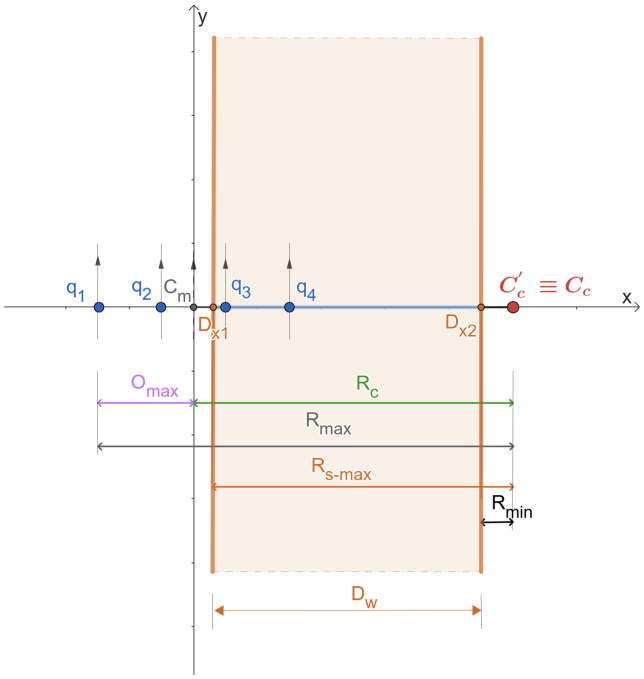

FIGURE 8. Feasible region on a straight path section with a clockwise direction of travel with an alongside formation.

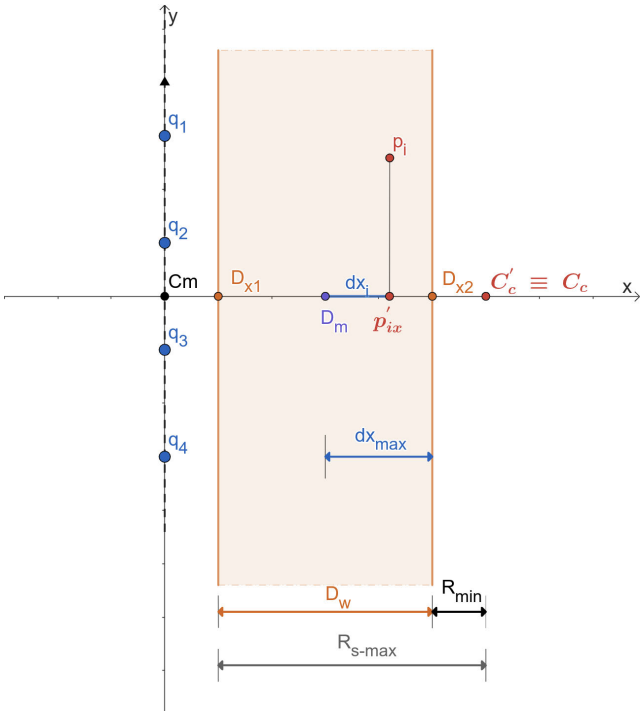

FIGURE 9. Feasible region on a straight section of a path and clockwise direction with single line formation.

Denoting by O_{max} the distance between C_m and the position of the outermost vehicle in formation, the radius of curvature of the outermost vehicle is given by:

$$R_{v_{max}} = R_c + O_{max} \tag{21}$$

Consider now that vehicles following the circular section with a larger radius of curvature move with a higher linear velocity. Indeed, in order to maintain the formation, the angular velocity ω_N along the circular section of a path must be the same for both target vehicles and sensors, and given the maximal speed limitation for both targets and sensors, we can derive the maximum radius of curvature (called $R_{s_{max}}$ in the following) that a sensor can have without exceeding such a limit. In the most common case, the targets are high-performance vehicles, while the sensors are low-performance vehicles, so the maximum speed of the targets is expected to be higher than that of the sensors ($v_{v_{max}} \geq v_{s_{max}}$). Let be $v_{v_{max}}$ the speed of the outermost vehicle, the maximum ω_N admissible for the formation is:

$$\omega_{N_{max}} = \frac{v_{v_{max}}}{R_{v_{max}}}, \tag{22}$$

and the maximum radius of curvature for the sensor compatible with its speed limit is given by:

$$R_{s_{max}} = \frac{v_{s_{max}}}{v_{v_{max}}} \cdot R_{v_{max}} \tag{23}$$

Hence, sensors positioned outside the orange region in Fig. 7, would follow a path with a radius of curvature greater than $R_{s_{max}}$, thus violating its speed limit. As a consequence, in the case of a counterclockwise direction of motion, sensors are constrained to lie on the left side of the formation.

Moreover, should the vehicles also have a maximal curvature limit due to physical constraints ($\omega_s \leq \omega_{s_{max}}$) of the platform, this results in a minimum radius of curvature $R_{min} = 1/\omega_{s_{max}}$ so as to avoid, for example, the vehicle rotating on the spot.

The analysis for finding the optimal position of the sensors is carried out considering the nominal system of targets and sensors at a generic time instant when the path is straight (figure 8). In order to derive the region of the feasible positions of the sensors, it is necessary to take also into account the paths of the targets and the sensors in the circular sections (figure 7). In particular, in light of the above considerations, we note how the feasible region for sensor positions has a width equal to $D_w = R_{s_{max}} - R_{min}$.

In the case of column formation (figure 9), all the considerations made so far are still valid. In this case all target vehicles travel on the same path and with the same speed.

In order to incorporate this constraint in the objective function, we adopt a solution similar to the one used for the communication constraint. We introduce a term in the FIM expression having the form of an appropriate sigmoid function.

Consider, without loss of generality, the sketch in figure 9. Let D_m be the midpoint of the two external points D_{x1} and D_{x2} of the feasible region represented in the figure. Let p'_{ix} denote the projection of the position of the generic $i-th$ sensor p_i on the $x-axis$, and let D_{max} be the maximum distance between D_m and for $i = 1, \ldots, n$, such that:

$$D^2_{max} = (D_w/2)^2.$$

Finally, define:

$$D^2_i = (p'_{ix} - D_m)^2, \tag{24}$$

so that the maximal speed constraint can be written as:

$$D^2_i \leq D^2_{max} \tag{25}$$

This allows translating the speed constraint into a geometric constraint on the sensor position. Again, the constraint is managed by adding a multiplicative term $s_{D^2_{max}}(D_i)$ in the FIM in eq. (12) having the form of a sigmoid function:

$$FIM_{c''}(q_j) = \frac{1}{\sigma^2} \sum_{i=1}^{n} s_{D^2_{max}}(D_i) FIM_{ij} \tag{26}$$

The parametric sigmoid term that allows to incorporate this latter constraint can be written as follows:

$$s_{D^2_{max}}(D_i) = \frac{1}{1 + e^{h(D^2_i - l)}} \tag{27}$$

with $i = 1, 2, \ldots, n$, where the parameters $h, l \in \mathbb{R}^+$ are function of D^2_{max} and determine the steepness, starting and ending point of the curve, and they can be tuned as previously described for the other constraints.

V. OBJECTIVE FUNCTION IN PRESENCE OF CONSTRAINTS

In this Section, we are now ready to define the objective function to solve the optimal sensor formation problem for multiple target positioning under the constraints discussed in the previous section.

As a first step, considering the $j-th$ target, we introduce in Eq. (12) the sigmoid terms associated to the addressed constraints, so as to obtain a properly weighted version of the FIM of $j-th$ target:

$$\overline{FIM}(q_j) = \frac{1}{\sigma^2} \sum_{i=1}^{n} s_{d_{max}}(r_{ij}) \cdot s_{d_{min}}(r_{ij}) \cdot s_{D^2_{max}}(D_i) \cdot \begin{bmatrix} \frac{(p_{ix}-q_{jx})^2}{r^2_{ij}} & \frac{(p_{ix}-q_{jx})(p_{iy}-q_{jy})}{r^2_{ij}} \\ \frac{(p_{ix}-q_{jx})(p_{iy}-q_{jy})}{r^2_{ij}} & \frac{(p_{iy}-q_{jy})^2}{r^2_{ij}} \end{bmatrix}, \tag{28}$$

with $i = 1, 2, \ldots, n$ and $j = 1, 2, \ldots, m$. For the ease of presentation, we use the following notations:

$$A_{ij} = \frac{(p_{ix} - q_{jx})}{r_{ij}}, \tag{29}$$

$$B_{ij} = \frac{(p_{iy} - q_{jy})}{r_{ij}}, \tag{30}$$

$$\varsigma_{ij} = s_{d_{max}}(r_{ij}) \cdot s_{d_{min}}(r_{ij}) \cdot s_{D^2_{max}}(D_i), \tag{31}$$

with $i = 1, 2, \ldots, n$ and $j = 1, 2, \ldots, m$. Thus, eq. (28) is rewritten in compact form as:

$$\overline{FIM}(q_j) = \frac{1}{\sigma^2} \sum_{i=1}^{n} \varsigma_{ij} \cdot \begin{bmatrix} (A_{ij})^2 & (A_{ij}B_{ij}) \\ (A_{ij}B_{ij}) & (B_{ij})^2 \end{bmatrix}. \tag{32}$$

The next step is to calculate the determinant of the matrix:

$$|\overline{FIM}(q_j)| = \frac{1}{\sigma^4} \left[\left(\sum_{i=1}^{n} \varsigma_{ij} \cdot A^2_{ij} \right) \cdot \left(\sum_{i=1}^{n} \varsigma_{ij} \cdot B^2_{ij} \right) - \left(\sum_{i=1}^{n} \varsigma_{ij} \cdot A_{ij} \cdot B_{ij} \right)^2 \right]. \tag{33}$$

Finally, we define the final objective function $\overline{\mathcal{F}}$ as:

$$\overline{\mathcal{F}} = \sum_{j=1}^{m} \ln(|\overline{FIM}(q_j)|). \tag{34}$$

so that, to obtain the optimal sensor configuration p for multiple target positioning in presence of all the constraints, we maximize the cost function in eq. (34):

$$\begin{aligned} p^* &= \arg\max_p(\ln(|\overline{FIM}(q_1)|) + \ldots + \ln(|\overline{FIM}(q_m)|)) \\ &= \arg\max_p \overline{\mathcal{F}}. \end{aligned} \tag{35}$$

Thus, the original problem is now recast into an unconstrained optimization problem, that it is now suited to be solved by resorting to the tools of numerical global optimization.

Before moving forward, we thoroughly analyze the objective function in order to identify the maximum accuracy that can be obtained in the localization of a single target.

In a general case, the solution of Eq. (35) may not be computable, however it is a trade-off among the maximum theoretical values obtained when each target is taken into account separately. Thus, in the following, we derive the maximum theoretical determinant of the FIM for the $j-th$ target, denoted as $|FIM_{MAX}(q_j)|$, which has the role of a helpful metric to evaluate the performance of the obtained trade-off solutions.

Let d_{jz} and d_{max} be, resp., the value of the depth of the $j-th$ target, and the maximum possible distance between target and sensor, and consider the circumference centered on the projection of the target on the plane where the sensors are located ($z=0$) having radius:

$$r_{max} = \sqrt{d_{max}^2 - d_{jz}^2}. \tag{36}$$

Exploiting the results in [12], it can be shown that the maximum theoretical determinant of the FIM for the $j-th$ target is obtained when:

$$FIM_{MAX}(q_j) = \frac{1}{\sigma^2}\begin{bmatrix} \frac{n}{2}\cdot\left(1-\frac{d_{jz}^2}{r_{max}^2}\right) & 0 \\ 0 & \frac{n}{2}\cdot\left(1-\frac{d_{jz}^2}{r_{max}^2}\right) \end{bmatrix}. \tag{37}$$

Therefore, the determinant of the $FIM_{MAX}(q_j)$ is:

$$|FIM_{MAX}(q_j)| = \frac{1}{\sigma^4}\cdot\frac{n^2}{4}\cdot\left(1-\frac{d_{jz}^2}{r_{max}^2}\right)^2. \tag{38}$$

The maximum theoretical value that the objective function in eq. (13) could reach is:

$$\mathcal{F}_{MAX} = \sum_{j=1}^{m}\ln(|FIM_{MAX}(q_j)|). \tag{39}$$

If all targets move on the same plane ($d_{jz}=d_z$):

$$|FIM_{MAX}| = \frac{1}{\sigma^4}\cdot\frac{n^2}{4}\cdot\left(1-\frac{d_z^2}{r_{max}^2}\right)^2, \tag{40}$$

$$\mathcal{F}_{MAX} = m\cdot\ln(|FIM_{MAX}|). \tag{41}$$

The values of the results expressed by the eq. (38 - 39) are used in the following as a benchmark to evaluate the performance of the results obtained in the presence of constraints, since $\mathcal{F}_{MAX}$ in eq. (39) takes into account only the communication constraint.

VI. SOLUTION OF THE UNCONSTRAINED OPTIMIZATION PROBLEM

In general, the objective function is non-convex and, for this reason, we adopt the Simulated Annealing algorithm [23], [24]. The advantage of this algorithm relies on the fact that it avoids being trapped in possible local minima, and it is able to reach the global optimal in a reduced computation time. Additionally, once that a solution is found using the Simulated Annealing algorithm, we refine the solution with the execution of a gradient-based optimization algorithm. In this way, we try to get as close as possible to the peak of the objective function. The steps of the overall algorithm are the following:

1) The positions of sensors p_i are initialized randomly;
2) The global optimization algorithm Simulated annealing is executed to obtain a first estimation of the optimal position p;
3) A Gradient Descent algorithm is carried out to refine the results obtained at point 2;
4) The feasibility of the sensors position obtained through the Gradient Descent algorithm is finally directly verified.

A first preliminary step is to define a reasonable range for the initial sensor positions. Figure 10 shows the domain of interest (denoted *DOMAIN* in the following). It is a rectangle with base D_w and height D_H, the base being equal to:

$$D_w = R_{s_{max}} - R_{min},$$

while the height depends on the mission and the path type. In the case under examination, we choose a value equal to:

$$D_H = 2\cdot R_{s_{max}}.$$

Defining the rectangular domain by the intervals along x and y, namely:

$$\begin{aligned} DOMAIN_x(x\text{-axis}): &\quad [D_{x1}, D_{x2}], \\ DOMAIN_y(y\text{-axis}): &\quad [-D_y, D_y]. \end{aligned}$$

For x-axis, if the direction of travel is clockwise we have:

$$\begin{cases} D_{x1} = R_{max} - R_{s_{max}} - O_{max} \\ D_{x2} = R_c - R_{min} \end{cases}, \tag{42}$$

and, if the direction of travel is counterclockwise we have:

$$\begin{cases} D_{x1} = -(R_c - R_{min}) \\ D_{x2} = -(R_{max} - R_{s_{max}} - O_{max}) \end{cases} \tag{43}$$

In both cases, for the y-axis, we have:

$$D_y = R_{s\_max} \tag{44}$$

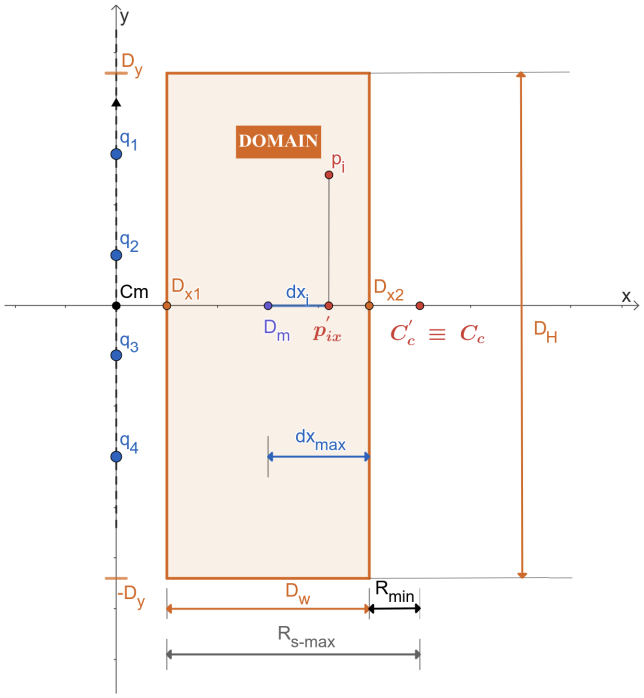

FIGURE 10. Domain in the straight section of a path and clockwise direction with vertical formation.

The pseudo-code of the first step is shown in the Algorithm 1, where the procedure *GenerateRandom* generates random numbers in the specified range with uniform distribution.

Algorithm 1 GenerateRandomGuess

Require: $n, R_c, R_{s\_max}, O_{max}, R_{min}, direction$
Ensure: $p, DOMAIN$
  $D_{x1} \leftarrow R_{max} - R_{s\_max} - O_{max}$
  $D_{x2} \leftarrow R_c - R_{min}$
  $D_y \leftarrow R_{s\_max}$
  if *direction* is clockwise **then**
    $DOMAIN_x \leftarrow [D_{x1}, D_{x2}]$
  else
    $DOMAIN_x \leftarrow [-D_{x2}, -D_{x1}]$
  end if
  $DOMAIN_y \leftarrow [-D_y, D_y]$
  for $i \leftarrow 1, 2, \ldots, n$ **do**
    $p_{ix} \leftarrow GenerateRandom(DOMAIN_x)$
    $p_{iy} \leftarrow GenerateRandom(DOMAIN_y)$
    $p_{iz} \leftarrow 0$
  end for

A. SIMULATION ANNEALING

The second step is the execution of the global optimization algorithm Simulated Annealing (SA) to obtain a rough estimation of the optimal position p. It uses randomness as part of the search process, and this makes the algorithm appropriate for nonlinear objective functions, especially when a desired global extremum is hidden among local extrema [25]. The core of the method of simulated annealing is an analogy with thermodynamics, specifically with the way that liquids freeze and crystallize, or metals cool and anneal. At high temperatures, the molecules of a liquid move freely with respect to one another. If the liquid is cooled slowly, thermal mobility is lost [26]. The essence of the Simulated Annealing is the following. Let be x a variable of interest and $f(x)$ an objective function. Start with an initial guess x, and compute the current $f(x)$. Then, x is perturbed randomly to $x_c = x + \Delta x$ and the objective function at the new point is calculated $f(x_c)$. If it is less/greater than the old value, the point is updated $x = x_c$. If, on the other hand, it is worse, it is accepted with a certain probability P using the "Metropolis" criterion:

$$P = e^{-\frac{\nabla f(x)}{T}}, \tag{45}$$

where

$$\nabla f(x) = f(x_c) - f(x)$$

is the difference between the current and the previous cost values, and the control parameter T represents the temperature, starting with an initial value and updating according to a cooling schedule, typically reducing it gradually over time. The above acceptance probability allows the algorithm to escape from local minima when the temperature is high. The effect is that poor solutions have more chances of being accepted early in the search and fewer chances of being accepted later in the search. The intent is that high temperatures in the early search help the algorithm locate the basin for the global optimum, while low temperatures in the late search help the algorithm refine the global optimum. However, it is important to note that the performance of simulated annealing heavily depends on the choice of the cooling schedule, perturbation operator, and other parameters specific to the problem domain.

There are several contributions where the multi-objective target problem is resolved through Simulated Annealing, some of them use Matlab optimization toolkit [13], and some others [14] use a different implementation. Nevertheless, the tools for SA used in literature, have some issues:

i. The Matlab's toolkit used in [13] is generic and it is not specialized for the particular problem at hand.
ii. The objective function proposed in [14] is similar to eq. (34) that is the sum of the logarithms of the FIM determinants. From a numerical point of view, this cost function could not significantly account for improvement or worsening since non-trivial worsening produces a very small difference. Therefore, there could be many poor updates, even if the temperature is very low.
iii. In [14], the chosen new points depend on the temperature because this allows us to consider an increasingly smaller search region. However, some solutions may not be evaluated as only certain areas of the domain are inspected. This causes the invalidation of the random component the Simulated Annealing is based on.

For these reasons, we implemented a properly tuned version of Simulated Annealing. To address the issue at point ii), the algorithm was executed considering a more numerically suitable objective function., as follows:

$$\overline{\mathcal{F}'} = \sum_{j=1}^{m} |\overline{FIM}(q_j)|. \tag{46}$$

It is the sum of the determinants of the FIM of the various targets and it produces more meaningful information when calculating the 'Metropolis' criterion.

Another significant ad-hoc adjustment is that the temperature is set low and constant for a certain number of initial iterations to increase the probability of approaching the optimal positioning. The new points are obtained by adding to the best point found a certain perturbation generated randomly, so that the current solution of the sensor $i-th$ denoted by pc_i results in:

$$\begin{cases} pc_{ix} = p_{ix} + \Delta p_{ix} \\ pc_{iy} = p_{iy} + \Delta p_{iy} \end{cases} \tag{47}$$

with Δp_{ix} and Δp_{iy} obtained as random values within $[lower_x, upper_x]$ and $[lower_y, upper_y]$, respectively, given by:

$$\begin{cases} lower_x = 0 \\ upper_x = abs(D_{x2} - D_{x1}) \\ lower_y = 0 \\ upper_y = abs(2 \cdot D_y) \end{cases} \tag{48}$$

If the numbers generated fall out of the domain (*DOMAIN* in figure 10), they are inserted starting from the opposite side. This is done by a recursive algorithm (algorithm 2) which ensures that the sensor position is actually in the correct region.

Algorithm 2 CheckBound

Require: $p_i, k, DOMAIN$
Ensure: p_i
▷ k is 0 if we check axis x, otherwise is 1 for y
▷ If it is out of range, it is reinserted in the opposite side
$stop \leftarrow DOMAIN_k[1]$
$start \leftarrow DOMAIN_k[0]$
if $p_i[k] > stop$ **then**
$diff \leftarrow abs(stop - p_i[k])$
$p_i[k] \leftarrow start + diff$
end if

Finally, the temperature is decreased by a parameter ΔT chosen to be small enough to ensure that the whole region is explored. T is initialized multiplying $R_{s_{max}}$ by a constant.

$$T = \alpha \cdot R_{s_{max}}.$$

The pseudo-code in Algorithm 3 makes explicit all the changes and customization made in the algorithm.

B. GRADIENT DESCENT

The next step is to use the results obtained with the "*Simulated annealing*" algorithm as initial guess for a "*Gradient descent*" algorithm. In this case, it is expected to be close to the optimal solution, and therefore the refinement is made in small steps to reach the peak of the function as closely as possible. Thus, the final solution is obtained using the following iterative gradient optimization algorithm.

1) Start with the SA solution.
2) Calculate the gradient at the current solution of the cost function $\overline{\mathcal{F}}$ in eq. (34) with respect to the $x-y$ coordinate of sensors (the z coordinates being set to $z=0$), namely $\frac{\partial \overline{\mathcal{F}}}{\partial p_{ix}}, \frac{\partial \overline{\mathcal{F}}}{\partial p_{iy}}, i = 1, 2, \ldots, n$.
3) Update the solution by taking a small step in the direction of the gradient through the rule:
$$p_i^{t+1} = p_i^t + \lambda \cdot \frac{\partial \overline{\mathcal{F}}(p^t)}{\partial p_i^t} \tag{49}$$
with $i = 1, 2, \ldots, n$, $t = 0, 1, \ldots$ the time step, and λ the learning rate which controls the size of the updates.
4) Repeat points 2 and 3 until one of the following stop criteria is met:
   - Objective function in $t+1$ step is less than the objective function in the previous step t
   - Maximum number of iterations is reached
   - Step size is smaller than the tolerance (due to scaling or a small gradient value).

The learning rate parameter λ is has an important role because it scales the gradient and it controls the step size. For this reason, it influences the performance of the algorithm and the quality of the result obtained. It is not easy to find a good value of λ a priori, but it is important to note the following potential drawbacks:

- **low learning rates** make the gradient converge slowly because the gradient has small updates.
- **high learning rates** make the gradient jump around the local maximum, and therefore never reach the optimal point.

For the problem at hand, the learning rate λ was set relatively low in order to carry out small update steps. For the execution of the gradient descent, the first derivatives of the cost function $\overline{\mathcal{F}}$ in Eq. (34) must be calculated.

C. FINAL REMARK

The pseudo-code of the whole proposed procedure to derive the optimal sensor formation is reported in Algorithm 4. The input parameters are: the position of the targets q in the local reference frame $\mathcal{O}$, the number of targets m, the number of sensors n, the direction of travel of the path *direction*, the radius of curvature of path R_c, the maximum speed for the targets and sensors, i.e. $v_{v_{max}}$ and $v_{s_{max}}$. The output of the algorithm is the position of the sensors p in the local reference frame $\mathcal{O}$.

As a final remark, in order to evaluate the performance of the proposed approach, we conducted an ablation study

Algorithm 3 SimulatedAnnealing

Require: $p, q, m, n, T_{min}, \alpha, a, b, f, g, h, l, DOMAIN$
Ensure: p
  $T \leftarrow \alpha \cdot R_{s\_max}$
  $(lower_x, lower_y) \leftarrow 0$
  $upper_x \leftarrow abs(DOMAIN_x[1] - DOMAIN_x[0])$
  $upper_y \leftarrow abs(DOMAIN_y[1] - DOMAIN_y[0])$
  $D_{mx} \leftarrow (DOMAIN_x[0] + DOMAIN_x[1])/2$
  $fim\_best \leftarrow CalculatedFIM(p, q, m, n, D_{mx})$
    ▷ Compute all $|\overline{FIM}(q_j)|$ by applying eq. (33)
  $TOTAL\_FIM \leftarrow SumFim(fim\_best, m)$
    ▷ Sum of all $|\overline{FIM}(q_j)|$ eq. (46)
  while $T > T_{min}$ **do**
    for $u \leftarrow 1, 2, \ldots, mc$ **do** ▷ mc: number of iteration in which the T is not decreased
      for $i \leftarrow 1, 2, \ldots, n$ **do**
        Compute pc_{ix} and pc_{iy} using eq.(47)
          ▷ Perturbation of the best point
        $CheckBound(pc_i, DOMAIN, 0)$
        $CheckBound(pc_i, DOMAIN, 1)$
          ▷ Ensure that the point falls in the $DOMAIN$
      end for
      $fim_c \leftarrow CalculatedFIM(pc, q, m, n, D_{mx})$
      $TOTAL\_FIM_c \leftarrow SumFim(fim_c, m)$
      $accept \leftarrow false$
      if $TOTAL\_FIM_c > TOTAL\_FIM$ **then**
        $accept \leftarrow true$
      else
        $delta = |TOTAL\_FIM_c - TOTAL\_FIM|$
        $condition = exp(-delta/T)$
        if $condition > rand()$ **then**
          ▷ Generate a random number ∈ [0, 1]
          $accept \leftarrow true$
        end if
      end if
      if $accept \leftarrow true$ **then**
        $TOTAL\_FIM \leftarrow TOTAL\_FIM_c$
        $p \leftarrow pc$
      end if
    end for
    $T \leftarrow T - \Delta T$
  end while
  return p

by systematically removing certain steps to understand the contribution of each component to the final optimal solution. In the proposed approach, once that the final objective function in eq. (34) is defined, the optimal solution is obtained by resorting to the global optimization algorithm Simulated annealing (SA) to find a close-to-optimal solution, followed by a Gradient descent (GD) algorithm to refine the solution. In particular, we carried out exhaustive experiments in which we calculated the optimal solution by excluding one of the two algorithms at a time. From this analysis, we have confirmed that the optimal solution obtained with only gradient descent can become trapped in local minima, leading to solutions that are worse. On the other hand, the use of the Simulated annealing alone leads to a close-to-optimal solution that can be further refined. It is worth mentioning that the computational time increases when both algorithms are considered, so the choice of the most suitable optimization strategy depends on the specific application at hand. Indeed, if a small computational time is required, such as in on-line applications, the use of the SA alone could be sufficient; in contrast, when a more accurate solution is required, the combination of SA and GD might be preferred.

Algorithm 4 FindSensorsPosition

Require: $q, m, n, direction, R_c, v_{v_{max}}, v_{s_{max}}$
Ensure: p
  $(a, b, h, l, f, g, R_{s\_max}, R_{min}, O_{max},) \leftarrow$
    $InitializeSigmoidParameters(q, v_{v_{max}}, v_{s_{max}}, R_c)$
  $(p_{guess}, DOMAIN) \leftarrow GenerateRandomGuess$
    $(n, R_c, R_{s\_max}, O_{max}, R_{min},$
  $direction)$
  Initialize T_{min} with a low value and $\alpha \epsilon [1, 5]$
  $p \leftarrow SimulatedAnnealing(p_{guess}, q, m, n, T_{min}, \alpha, a, b,$
  $f, g, h, l, DOMAIN)$
  $p \leftarrow ExecuteGradient(p, q, m, n, a, b, h, l, f, g)$
  return p

VII. NUMERICAL SIMULATIONS IN A 3D SCENARIO

This Section describes the numerical simulations of the proposed algorithm. The algorithm is coded using the 'C++' programming language and is integrated into the 'Robot Operating System' (ROS) middle-ware. In this section we focus on the results of numerical simulations. The purpose is to identify the optimal positioning of the sensors according to the operating conditions. Tests are performed with an 'Intel core i7-10700k @ 3.80GHz CPU' using 'Ubuntu 22.10' as OS.

A. DEFINITION OF THE MISSION SCENARIO

The algorithm proposed in the previous section is tested considering a real mission scenario with multiple vehicles. The mission features are defined through a set of input parameters that specify the required operating conditions. In a real scenario, these mission parameters could be defined by the user. It is assumed that the positions of the targets are not specified explicitly, but an area of feasibility, in terms of length and width, is assigned. The center of the formation C_m is located in the specified area's center. Targets are then arranged according to the specified type of formation, thus the distance between adjacent target vehicles, denoted as *offset* in the following, is a function of the formation's length and width. The considered input parameters are reported in Table 1.

The operating depth of the targets is assumed to be a value known in advance; without loss of generality, in simulation,

TABLE 1. Input parameters for the definition of mission scenario.

INPUT	
Parameter	**Description**
m	number of targets
n	number of sensors
DIRECTION	direction along the path: *'clockwise'*; *'counterclockwise'*
FORMATION	type of formation
LENGTH	length of the region related to target formation
WIDTH	width of the region related to target formation
RADIUS	curvature radius of the planned path
$v_{v_{max}}$	maximum speed of the targets
$v_{s_{max}}$	maximum speed of the sensors
DEPTH	operating target depth

it is set equal to 50 m for each vehicle.

$$q_{jz} = d_z = 50 \text{ m with } j = 1, 2, \ldots, m.$$

Other quantities required for the execution of the algorithm concern the constraints:

- d_{max}: maximum distance between a sensor and a target. In simulations, d_{max} is set to

$$d_{max} = 1000 \text{ m},$$

  with parameters $a = 1.22$ and $b = 995.25$ for the sigmoid s_{dmax}.
- d_{min}: minimum distance between the sensor and the target/sensor. This parameter can be set, for example, equal to the distance between two adjacent vehicles (*offset*).
- dx_{max}: maximum distance between the projection of the position of the sensor p_i on the x-axis p'_{ix} and D_m. This parameter allows the constraint on the maximum speed limit of the sensors to be satisfied. The value of this parameter is obtained dynamically during the execution of the algorithm and depends on the value of the input parameters defined by the mission scenario.

In addition, the other mission parameters are:

- σ: standard deviation of the measurement error.
- T: temperature used in the execution of the simulated annealing algorithm.
- T_{min}: exit condition of the simulated annealing algorithm. When T becomes equal to or less than the value of this parameter, the algorithm stops execution.
- ΔT: parameter that represents how much the temperature decreases at each iteration.
- **mc**: number of iterations to be performed before the temperature decreases.

TABLE 2. Parameters required for the execution of the algorithm.

Parameter	Value	Description
d_{max}	1000 m	maximum distance possible between sensor and target
d_{min}	*offset* (m)	minimum distance possible between target and sensor. Offset is the distance between two contiguous targets
dx_{max}	$D_w/2$ (m)	maximum possible distance between p'_{ix} and D_m
σ	0.1 m	standard deviation in measurement error
T	$2 \cdot R_{s_{max}}$	temperature T used in Simulated Annealing
ΔT	0.05	how temperature T decrease during SA execution
T_{min}	0.00001	exit condition for SA
mc	5	iterations before the temperature decrease
$maxIte$	8000000	maximun number of iteration in gradient descent algorithm
λ	0.001	learning rate

- λ: learning rate in the execution of the gradient descent algorithm.
- **maxIte**: maximum iteration number of the gradient descent algorithm.

Table 2 shows the values assumed by each of these parameters during the tests carried out.

We are now ready to show the simulation results provided by the proposed optimal sensor formation procedure in different operating mission scenarios to evaluate its performance.

1) EXAMPLE 1: $m = 6$, $n = 4$, CLOCKWISE

A first numerical example is here reported. The input parameters for this mission scenario are presented in table 3. Table 4 shows the nominal target formation in frame $\mathcal{F}$ in accordance with the chosen input parameters, while figure 11 graphically represents the corresponding feasible sensor deployment area. In order to evaluate the performance of the solution that we obtain with the proposed algorithm for optimal sensor formation, we derive the maximum theoretical performance achievable for the considered scenario. The maximum theoretical *FIM* determinant value achievable from a single target, given by eq. (40), is:

$$|FIM_{MAX}| = 39799.75 \text{ m}^{-4}, \tag{50}$$

while the corresponding maximum value achievable by the objective function, given by eq. (41), is:

$$\mathcal{F}_{MAX} = 63.55 \text{ m}^{-4}. \tag{51}$$

Applying the proposed optimal sensor formation procedure in Algorithm 4, we obtain the solution given in Table 5 and illustrated in figure 12.

TABLE 3. Input parameters for Example 1.

INPUT	
Parameter	**Value**
m	6
n	4
DIRECTION	clockwise
FORMATION	alongside
LENGTH	600 m
WIDTH	500 m
RADIUS	600 m
$v_{v_{max}}$	1 m/s
$v_{s_{max}}$	0.7 m/s

TABLE 4. Nominal target formation in frame $\mathcal{F}$ for Example 1.

TARGET $\mathbf{q}$(m)			
	x	y	z
$\mathbf{q}_1$	250.00	0.00	50.00
$\mathbf{q}_2$	150.00	0.00	50.00
$\mathbf{q}_3$	50.00	0.00	50.00
$\mathbf{q}_4$	-50.00	0.00	50.00
$\mathbf{q}_5$	-150.00	0.00	50.00
$\mathbf{q}_6$	-250.00	0.00	50.00

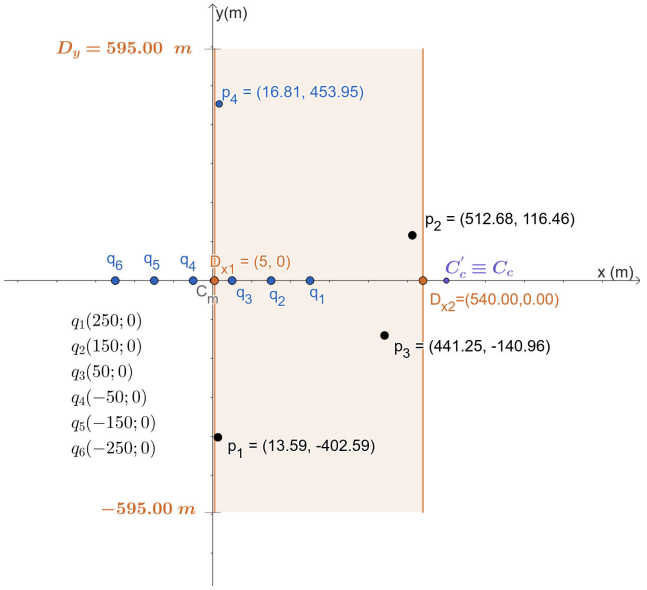

FIGURE 11. Feasible sensor deployment area for Example 1.

TABLE 5. Mission compliant optimal sensor formation in $\mathcal{O}$ for Example 1.

SENSOR $\mathbf{p}$(m)			
	x	y	z
$\mathbf{p}_1$	13.59	−402.59	0.000000
$\mathbf{p}_2$	512.68	116.46	0.000000
$\mathbf{p}_3$	441.25	−140.96	0.000000
$\mathbf{p}_4$	16.81	453.95	0.000000

Table 6, displays some parameters values obtained in the execution of Algorithm 4: The final objective function incorporating the presence of constraints has the value:

$$\overline{\mathcal{F}} = 63.33\ \text{m}^{-4}.$$

Table 7 shows the determinants of FIMs with respect to each target. The smallest value obtained is $|\overline{FIM}(q_6)| = 36940.07\ \text{m}^{-4}$. Thus, the degradation with respect to the maximum theoretical value obtainable from a single target is:

$$\varrho_{min\_|\overline{FIM}|} = 100 - \frac{36940.07 \cdot 100}{39799.75} = 7.19\%,$$

while the degradation of the value of the final objective function found with respect to the theoretical one is:

$$\varrho_{\overline{\mathcal{F}}} = 100 - \frac{63.33 \cdot 100}{63.55} = 0.35\%.$$

We can see how the degradation due to the presence of constraints and multiple targets is limited, and the results obtained are close to the maximum theoretical values achievable.

Furthermore, Figure 13 shows the level curves in 2D and 3D of the objective function incorporating the presence of constraints for each $\{x - y\}$ point computed as if there were a hypothetical target at that point. They show how the maximum values are over the region containing the targets.

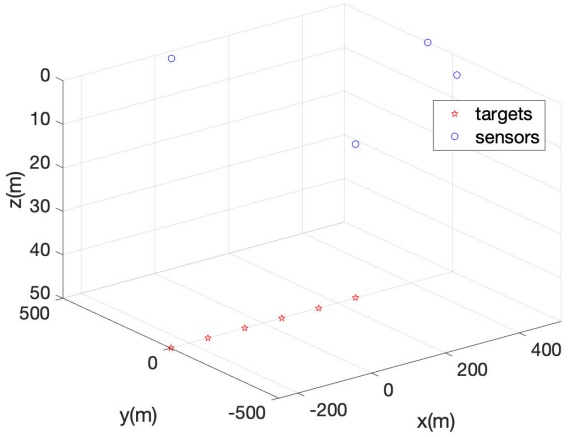

FIGURE 12. Mission-compliant optimal sensor formation for Example 1.

TABLE 6. Parameters of interest for the Example 1.

Parameters of interest	
Parameter	**Value**
offset	100.00 m
O_{max}	250.00 m
R_{max}	850.00 m
$R_{s_{max}}$	595.00 m
R_{min}	60.00 m
D_{x1}	5.00 m
D_{x2}	540.00 m
D_y	595.00 m
D_w	535.00 m
d_{min}	100.00 m
dx_{max}	267.5 m
f	12.19
g	99.38
h	0.017035
l	71216.35

2) EXAMPLE 2: $m = 6$, $n = 3$, COUNTERCLOCKWISE

A second example is considered whose mission input parameters are reported in Table 8. Table 9 shows the nominal target formation in frame $\mathcal{F}$ in accordance with

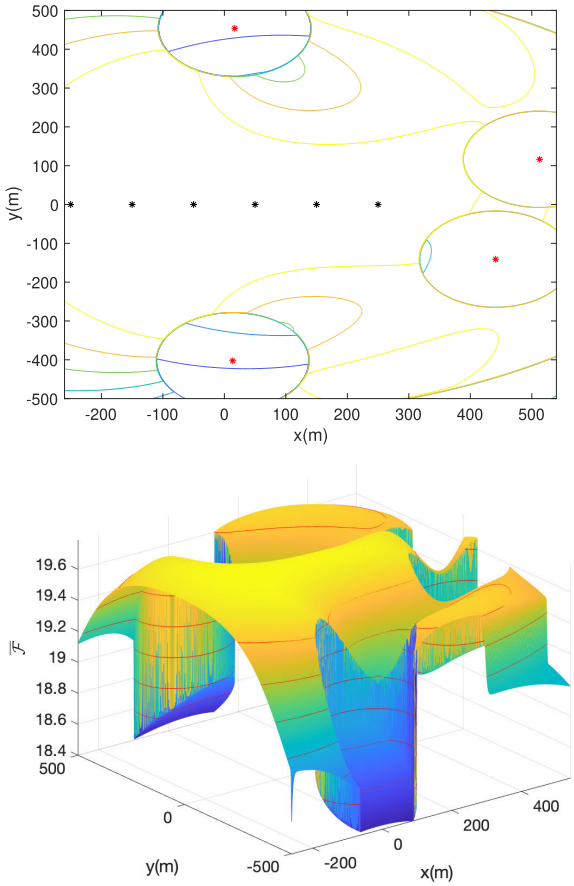

FIGURE 13. Level curves in 2D (top) and 3D (bottom) of the objective function for Example 1.

TABLE 7. Determinant of $\overline{FIM}$ for each target for Example 1 considering the presence of mission constraints.

$\lvert\overline{FIM}\rvert$ (m^{-4})	
j	$\lvert\overline{FIM}(\mathbf{q}_j)\rvert$
$\lvert\overline{FIM}(\mathbf{q}_1)\rvert$	38083.32
$\lvert\overline{FIM}(\mathbf{q}_2)\rvert$	38559.83
$\lvert\overline{FIM}(\mathbf{q}_3)\rvert$	38674.43
$\lvert\overline{FIM}(\mathbf{q}_4)\rvert$	39033.14
$\lvert\overline{FIM}(\mathbf{q}_5)\rvert$	38900.34
$\lvert\overline{FIM}(\mathbf{q}_6)\rvert$	36940.07

these input parameters, while figure 14 graphically shows the corresponding feasible sensor deployment area. Opposite to the previous Example, the left side of the potential sensor area is considered due to the counterclockwise direction of motion.

From eq. (40), we can evaluate the maximum theoretical *FIM* determinant value achievable from a single target for the considered scenario, that is:

$$|FIM_{MAX}| = 22387.36 \text{ m}^{-4}, \tag{52}$$

TABLE 8. Input parameters for Example 2.

INPUT	
Parameter	**Value**
m	6
n	3
DIRECTION	counterclockwise
FORMATION	alongside
LENGTH	750 m
WIDTH	400 m
RADIUS	800 m
$v_{v_{max}}$	1 m/s
$v_{s_{max}}$	0.75 m/s

TABLE 9. Nominal target formation in frame $\mathcal{O}$ for Example 2.

TARGET $\mathbf{q}$ (m)			
	x	y	z
$\mathbf{q}_1$	312.50	0.00	50.00
$\mathbf{q}_2$	187.50	0.00	50.00
$\mathbf{q}_3$	62.50	0.00	50.00
$\mathbf{q}_4$	-62.50	0.00	50.00
$\mathbf{q}_5$	-187.50	0.00	50.00
$\mathbf{q}_6$	-312.50	0.00	50.00

while the corresponding maximum value achievable by the objective function (eq. (41)) is:

$$\mathcal{F}_{MAX} = 60.10 \text{ m}^{-4}. \tag{53}$$

Applying the proposed optimal sensor formation procedure in Algorithm 4, we obtain the solution given in Table 10 and illustrated in figure 15.

The final objective function incorporating the presence of constraints has the value:

$$\overline{\mathcal{F}} = 59.73 \text{ m}^{-4}.$$

Table 12 shows the determinants of *FIMs* with respect to each target. The smallest value obtained is $|\overline{FIM}(q_3)| = 19821.08 \text{ m}^{-4}$. Thus, the degradation with respect to the maximum theoretical value obtainable is:

$$\varrho_{min\_|\overline{FIM}|} = 100 - \frac{19821.08 \cdot 100}{22387.36} = 11.5\%,$$

while the degradation of the value of the objective function with respect to the theoretical one is:

$$\varrho_{\overline{\mathcal{F}}} = 100 - \frac{59.73 \cdot 100}{60.10} = 0.6\%.$$

As expected, the performance obtained in this scenario are slightly lower, compared to the previous example, due to the presence of a reduced number of sensors. Nevertheless, the overall degradation with respect to the maximum theoretical values is still limited, so results are satisfactory.

Table 11 shows the values of some parameters of interest obtained in the execution the algorithm:

VIII. UNCERTAINTY IN THE TARGET LOCATIONS

In previous Sections we implicitly assumed that the target positions were exactly known even before positioning the sensors in their optimal formation. However, in real-world

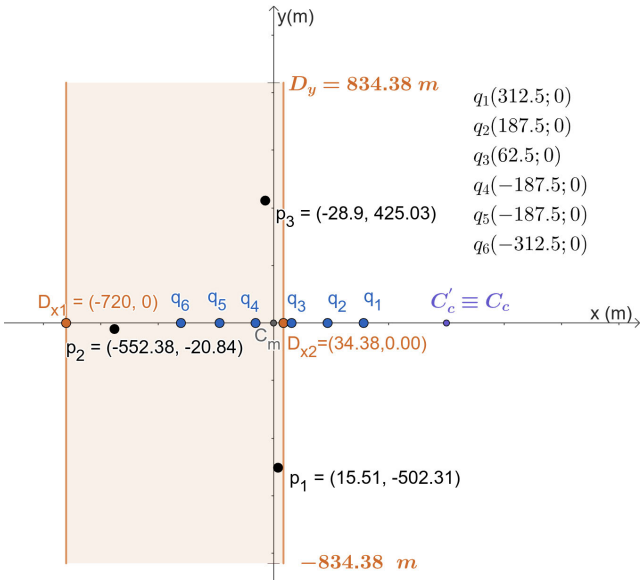

FIGURE 14. Feasible sensor deployment area for Example 2.

TABLE 10. Optimal sensor formation for Example 2 considering the presence of mission constraints.

	SENSOR p (m)		
	x	y	z
$\mathbf{p}_1$	15.51	−502.31	0.000000
$\mathbf{p}_2$	−552.38	−20.84	0.000000
$\mathbf{p}_3$	−28.90	425.03	0.000000

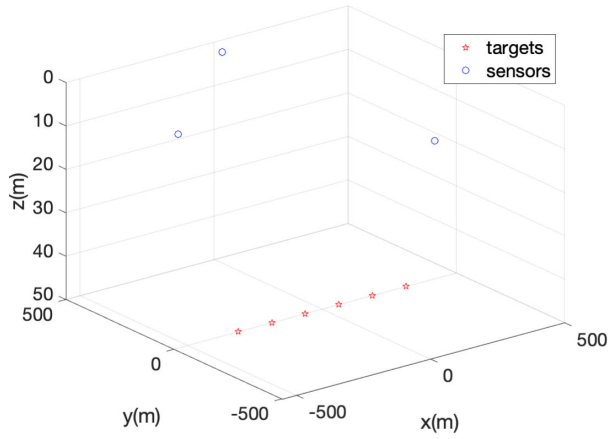

FIGURE 15. Mission-compliant optimal sensor formation for Example 2.

scenarios, a depth sensor can precisely provide the target's depth, but the target's position in the $x-y$ plane is typically known with some uncertainty (see figure 16). The approach that we take to address this practical problem is inspired by the set-up described in [11] and [20] where each target is assumed to lie in a well-defined region of uncertainty, characterized by a proper probability density function (PDF). The objective is to derive the optimal sensor formation taking explicitly into account an uncertainty in the target location. The formulation of the problem discussed in Section III still holds.

TABLE 11. Parameters of interest for Example 2.

Parameters of interest	
Parameter	Value
$offset$	125.00 m
O_{max}	312.50 m
R_{max}	1112.50 m
R_{s_max}	834.38 m
R_{min}	80.00 m
D_{x1}	−720.00 m
D_{x2}	34.38 m
D_y	834.38 m
D_w	754.38 m
d_{min}	125.00 m
dx_{max}	377.19 m
f	9.75
g	124.22
h	0.008568
l	141594.61

TABLE 12. Determinant of $\overline{FIM}$ for each target for Example 2 considering the presence of mission constraints.

$\lvert\overline{FIM}\rvert$ (m^{-4})	
j	$\lvert\overline{FIM}(q_j)\rvert$
$\lvert\overline{FIM}(q_1)\rvert$	21980.28
$\lvert\overline{FIM}(q_2)\rvert$	21747.54
$\lvert\overline{FIM}(q_3)\rvert$	20058.95
$\lvert\overline{FIM}(q_4)\rvert$	19821.08
$\lvert\overline{FIM}(q_5)\rvert$	21322.70
$\lvert\overline{FIM}(q_6)\rvert$	21501.85

A. PROBLEM DESCRIPTION

Let D_j be the distribution area of the $j-th$ vehicle and $\varphi(q_j)$ its probability density function. In practical applications, $\varphi(q_j)$ depends on the prior knowledge of the target locations and on their mission, and different distributions can be taken into account, as for example the uniform distribution within the area. Regardless the specific PDF to be considered, we can define the objective function as follows:

$$\overline{\mathcal{F}}^{unc} = \sum_{j=1}^{m} \ln\left(\int_{D_j} |\overline{FIM}(q_j)|\varphi(q_j)dq_j\right) \tag{54}$$

This is equivalent to maximize, by proper sensor formation, the average value of the FIM determinant in presence of constraints for the uncertainty region of the target location. A similar approach, although with a different objective function that does not take into account any constraints, has also been proposed in [14]. In this case, we opt for a numerical computation of the integral in eq. (54) over the uncertainty region using a Monte Carlo method. The final objective function exploits the numerical Monte Carlo computation of integral in Eq. (54)) and it is given by:

$$\overline{\mathcal{F}}^{unc} \approx \sum_{j=1}^{m} \ln\left(\frac{1}{k}\sum_{v=1}^{k} |\overline{FIM}(q_{jv})|\right) \tag{55}$$

where k is the number of hypothetical targets in different locations in an uncertain area, as shown by the blue dots

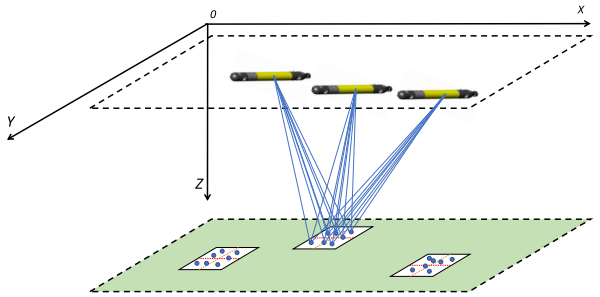

FIGURE 16. Uncertainty in the target locations.

in figure 16. The computation of $\overline{\mathcal{F}}^{unc}$ is made through Algorithm 5.

Algorithm 5 CalculateUncertaintyFim

Require: $\bar{q}, p, m, n, \sigma, \sigma_q$
Ensure: $|\overline{FIM}^{unc}_{TOT}|$
  $|\overline{FIM}^{unc}_{TOT}| \leftarrow 0$
  for $j \leftarrow 1, 2, \ldots, m$ **do**
    $|FIM(q_j)| \leftarrow 0$
    for $v \leftarrow 1, 2, \ldots, k$ **do** ▷ k is the number of $j-th$ target points generated
      $q_j \leftarrow GenerateRandomPoints(\bar{q}_j, \sigma_q)$ ▷ The function "GenerateRandomPoints" generates the position q_j with a pseudo random number generator with uniform or Gaussian distribution
      $|FIM(q_j)| \leftarrow |FIM(q_j)| + CalculateFIM(q_j, p, m, n, \sigma)$
      ▷ At each iteration v the $|FIM(q_j)|$ is calculated given the generated position q_j
    end for
    $|FIM(q_j)| \leftarrow |FIM(q_j)|/k$
    $|\overline{FIM}^{unc}_{TOT}| \leftarrow |\overline{FIM}^{unc}_{TOT}| + |FIM(q_j)|$
  end for

B. NUMERICAL SIMULATION

In this Section, we provide a final example of multiple sensor placement when the positions of the targets are known with uncertainty.

We assume that the PDF of each $j-th$ target has a Gaussian distribution, where the mean $\bar{q}$ and standard deviation σ_q of targets q are known. The standard deviation σ_q is set equal to 3 m for all of them. Parameter k is set to 1000.

1) EXAMPLE: $m = 6$, $n = 2$, COUNTERCLOCKWISE

The input parameters of the mission scenario are reported in table 13, while table 14 shows the mean $\bar{q}_j$ of the distributions of the target positions in frame $\mathcal{F}$.

From equation (40), the maximum theoretical *FIM* determinant value achievable from a single target is:

$$|FIM_{MAX}| = 9949.94 \text{ m}^{-4}, \tag{56}$$

TABLE 13. Input parameters.

INPUT	
Parameter	**Value**
m	6
n	2
DIRECTION	counterclockwise
FORMATION	single line
LENGTH	300 m
WIDTH	700 m
RADIUS	750 m
$v_{v_{max}}$	1.2 m/s
$v_{s_{max}}$	0.9 m/s

TABLE 14. Means $\bar{q}_j$ of the distributions of the target positions in frame $\mathcal{F}$.

TARGET $\bar{q}$ (m)			
	x	**y**	**z**
$\bar{q}_1$	0.00	291.67	50.00
$\bar{q}_2$	0.00	175.00	50.00
$\bar{q}_3$	0.00	58.33	50.00
$\bar{q}_4$	0.00	-58.33	50.00
$\bar{q}_5$	0.00	-175.00	50.00
$\bar{q}_6$	0.00	-291.67	50.00

TABLE 15. Optimal sensor formation.

SENSOR p (m)			
	x	**y**	**z**
$\mathbf{p}_1$	−379.85	−554.25	0.000000
$\mathbf{p}_2$	−578.31	495.21	0.000000

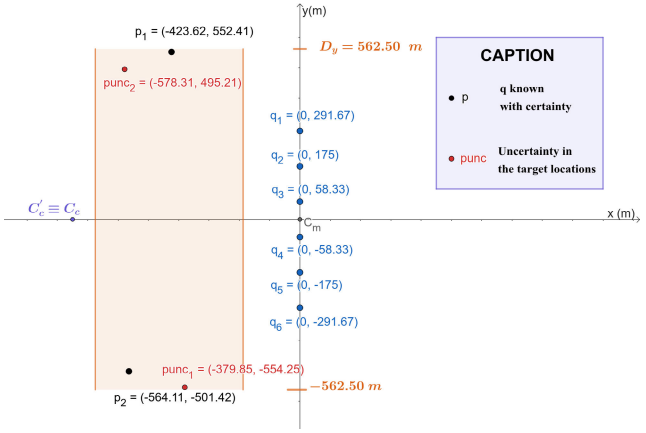

FIGURE 17. Feasible region of the sensor positions.

while the corresponding maximum value achievable by the objective function, given by eq. (41) is:

$$\mathcal{F}_{MAX} = 55.23 \text{ m}^{-4} \tag{57}$$

Applying the proposed optimal sensor formation procedure in Algorithm 5 (from algorithm 4), we obtain the solution given in Table 15 and illustrated in figure 17.

Table 16 shows the values of some parameters of interest obtained in the execution of the algorithm. The final objective function has the value:

$$\overline{\mathcal{F}}^{unc} = 55.16 \text{ m}^{-4}.$$

TABLE 16. Parameters of interest for the example.

Quantities of interest	
Parameter	**Value**
$offset$	116.67 m
O_{max}	0.00 m
R_{max}	750.00 m
R_{s_max}	562.50 m
R_{min}	75.00 m
D_{x1}	−675.00 m
D_{x2}	−187.50 m
D_y	562.50 m
D_w	487.50 m
d_{min}	116.67 m
dx_{max}	243.75 m
f	10.45
g	115.94
h	0.02
l	59131.83

TABLE 17. Determinant of FIM for each target for the example.

$\lvert\overline{FIM}^{unc}\rvert$ (m^{-4})	
j	$\lvert\overline{FIM}^{unc}(q_j)\rvert$
$\lvert\overline{FIM}^{unc}(q_1)\rvert$	9836.45
$\lvert\overline{FIM}^{unc}(q_2)\rvert$	9899.69
$\lvert\overline{FIM}^{unc}(q_3)\rvert$	9820.49
$\lvert\overline{FIM}^{unc}(q_4)\rvert$	9778.35
$\lvert\overline{FIM}^{unc}(q_5)\rvert$	9830.44
$\lvert\overline{FIM}^{unc}(q_6)\rvert$	9849.47

Table 17 shows the determinants of FIMs with respect to each target. The smallest value obtained is $\lvert\overline{FIM}^{unc}(q_4)\rvert = 9778.35 \ \ \mathrm{m}^{-4}$, so the degradation with respect to the maximum theoretical value obtainable is:

$$\varrho_{min\_\lvert\overline{FIM}\rvert} = 100 - \frac{9778.35 \cdot 100}{9949.94} = 1.72\%$$

The degradation of the value of the objective function with respect to the theoretical one is:

$$\varrho_{\overline{\mathcal{F}}^{unc}} = 100 - \frac{55.16 \cdot 100}{55.23} = 0.13\%.$$

We can see how the degradation is very limited. The values obtained inside the uncertainty areas are very close to the maximum theoretical ones. Figure 17 shows the optimal positions of the sensors in both cases: when the target positions are known with uncertainty, and with certainty. In this specific case, the results obtained are symmetric with respect to the x-axis, so they havenearly the same distance from the targets. Nevertheless, the solution obtained using the objective function in Eq. (55) is, by construction, more robust with respect to uncertainty in the knowledge of nominal target locations.

IX. CONCLUSION

This paper addresses the problem of the optimal sensor formation for range-based underwater localization of a team of vehicles moving in formation. We propose a solution that may be used as a pre-planning tool in realistic and practical mission scenarios. Despite the approaches usually adopted, we explicitly take into account constraints imposed by the mission that restrict the feasible sensor deployment area, such as communication constraints, safety constraints, and maximal vehicle speed limitations. The problem is formulated by resorting to estimation theory tools. In particular, we recast the problem as an unconstrained optimization problem where all constraints are incorporated into a properly shaped objective function based on the Fisher Information Matrix. This allows using a simulated annealing optimization algorithm to define the optimal sensor formation. Finally, we address the more realistic scenario where the positions of the targets are known with some uncertainty. Several numerical simulations have been performed, considering different configurations with an arbitrary number of sensors and targets, confirming the effectiveness of the proposed approach. Future extensions of this work are currently in progress to adapt the approach to arbitrary motion trajectories, beyond just circular or racecourse paths. Furthermore, future work will focus on an experimental campaign to verify the effectiveness of the approach in a real-world multiple vehicle mission scenario.

REFERENCES

[1] G. Antonelli, F. Arrichiello, A. Caiti, G. Casalino, D. De Palma, G. Indiveri, M. Razzanelli, L. Pollini, and E. Simetti, "ISME activity on the use of autonomous surface and underwater vehicles for acoustic surveys at sea," *ACTA IMEKO*, vol. 7, no. 2, pp. 24–31, Jul. 2018.

[2] B. Allotta, G. Antonelli, A. Bongiovanni, A. Caiti, R. Costanzi, D. De Palma, P. Di Lillo, M. Franchi, P. Gjanci, G. Indiveri, C. Petrioli, A. Ridolfi, and E. Simetti, "Underwater acoustic source localization using a multi-robot system: The DAMPS project," in *Proc. Int. Workshop Metrol. Sea, Learn. Measure Sea Health Parameters (MetroSea)*, Oct. 2021, pp. 388–393.

[3] Y. Wu, K. H. Low, and C. Lv, "Cooperative path planning for heterogeneous unmanned vehicles in a search-and-track mission aiming at an underwater target," *IEEE Trans. Veh. Technol.*, vol. 69, no. 6, pp. 6782–6787, Jun. 2020.

[4] L. Paull, S. Saeedi, M. Seto, and H. Li, "AUV navigation and localization: A review," *IEEE J. Ocean. Eng.*, vol. 39, no. 1, pp. 131–149, Jan. 2014.

[5] X. Bo, A. A. Razzaqi, and G. Farid, "A review on optimal placement of sensors for cooperative localization of AUVs," *J. Sensors*, vol. 2019, Jul. 2019, Art. no. 4276987, doi: 10.1155/2019/4276987.

[6] W. A. P. van Kleunen, K. C. H. Blom, N. Meratnia, A. B. J. Kokkeler, P. J. M. Havinga, and G. J. M. Smit, "Underwater localization by combining time-of-flight and direction-of-arrival," in *Proc. OCEANS*, Apr. 2014, pp. 1–6.

[7] T. Alexandri, M. Walter, and R. Diamant, "A time difference of arrival based target motion analysis for localization of underwater vehicles," *IEEE Trans. Veh. Technol.*, vol. 71, no. 1, pp. 326–338, Jan. 2022.

[8] J. S. Abel, "Optimal sensor placement for passive source localization," in *Proc. Int. Conf. Acoust., Speech, Signal Process.*, Apr. 1990, pp. 2927–2930.

[9] S. Martínez and F. Bullo, "Optimal sensor placement and motion coordination for target tracking," *Automatica*, vol. 42, no. 4, pp. 661–668, Apr. 2006, doi: 10.1016/j.automatica.2005.12.018.

[10] A. N. Bishop, B. Fidan, B. D. O. Anderson, K. Doğançay, and P. N. Pathirana, "Optimality analysis of sensor-target localization geometries," *Automatica*, vol. 46, no. 3, pp. 479–492, Mar. 2010. [Online]. Available: https://www.sciencedirect.com/journal/automatica/vol/46/issue/3

[11] D. Moreno-Salinas, A. Pascoal, and J. Aranda, "Optimal sensor placement for multiple target positioning with range-only measurements in two-dimensional scenarios," *Sensors*, vol. 13, no. 8, pp. 10674–10710, Aug. 2013, doi: 10.3390/s130810674.

[12] D. Moreno-Salinas, A. Pascoal, and J. Aranda, "Optimal sensor placement for acoustic underwater target positioning with range-only measurements," *IEEE J. Ocean. Eng.*, vol. 41, no. 3, pp. 620–643, Jul. 2016.
[13] D. Moreno-Salinas, A. M. Pascoal, and J. Aranda, "Multiple underwater target positioning with optimally placed acoustic surface sensor networks," *Int. J. Distrib. Sensor Netw.*, vol. 14, no. 5, May 2018, Art. no. 155014771877323.
[14] B. Xu, X. Wang, A. A. Razzaqi, and X. Zhang, "Topology optimisation method for MACL formation based on acoustic measurement network," *IET Radar, Sonar Navigat.*, vol. 13, no. 6, pp. 927–936, Jun. 2019, doi: 10.1049/iet-rsn.2018.5384.
[15] M. Sadeghi, F. Behnia, and R. Amiri, "Optimal sensor placement for 2-D range-only target localization in constrained sensor geometry," *IEEE Trans. Signal Process.*, vol. 68, pp. 2316–2327, 2020.
[16] M. Sadeghi, F. Behnia, and R. Amiri, "Optimal geometry analysis for TDOA-based localization under communication constraints," *IEEE Trans. Aerosp. Electron. Syst.*, vol. 57, no. 5, pp. 3096–3106, Oct. 2021, doi: 10.1109/TAES.2021.3069269.
[17] S. Xu, M. Rice, and F. Rice, "Optimal TOA-sensor placement for two target localization simultaneously using shared sensors," *IEEE Commun. Lett.*, vol. 25, no. 8, pp. 2584–2588, Aug. 2021, doi: 10.1109/LCOMM.2021.3083058.
[18] X. Fang, J. Li, S. Zhang, W. Chen, and Z. He, "Optimal AOA sensor-source geometry with deployment region constraints," *IEEE Commun. Lett.*, vol. 26, no. 4, pp. 793–797, Apr. 2022.
[19] M. Villa, B. Ferreira, and N. Cruz, "Genetic algorithm to solve optimal sensor placement for underwater vehicle localization with range dependent noises," *Sensors*, vol. 22, no. 19, p. 7205, Sep. 2022, doi: 10.3390/s22197205.
[20] J. T. Isaacs, D. J. Klein, and J. P. Hespanha, "Optimal sensor placement for time difference of arrival localization," in *Proc. 48th IEEE Conf. Decis. Control (CDC), 28th Chin. Control Conf.*, Shanghai, China, Dec. 2009, pp. 7878–7884, doi: 10.1109/CDC.2009.5399478.
[21] Y. Bar-Shalom, X.-R. Li, and T. Kirubarajan, *Estimation With Applications to Tracking and Navigation*. New York, NY, USA: Wiley, 2001.
[22] S. Sharma, S. Sharma, and A. Athaiya, "Activation functions in neural networks," *Towards Data Sci.*, vol. 6, no. 12, pp. 310–316, 2017.
[23] R. A. Rutenbar, "Simulated annealing algorithms: An overview," *IEEE Circuits Devices Mag.*, vol. 5, no. 1, pp. 19–26, Jan. 1989.
[24] D. Bertsimas and J. Tsitsiklis, "Simulated annealing," *Stat. Sci.*, vol. 8, no. 1, pp. 10–15, Feb. 1993, doi: 10.1214/ss/1177011077.
[25] L. Ingber, "Adaptive simulated annealing (ASA): Lessons learned," *J. Control Cybern.*, vol. 25, no. 1, pp. 33–54, 1995. [Online]. Available: https://www.ingber.com/asa96_lessons.ps.gz
[26] W. H. Press, S. A. Teukolsky, W. T. Vetterling, and B. P. Flannery, *Numerical Recipes in C*, 2nd ed. Cambridge, MA, USA: Cambridge Univ. Press, 1992.

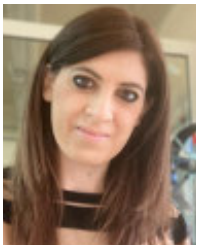

DANIELA DE PALMA received the M.Sc. degree (Hons.) in automation engineering from the University of Salento, Lecce, Italy, in 2008, and the Ph.D. degree in information engineering, in 2017. Since 2021, she has been a member of the Interuniversity Center of Integrated Systems for the Marine Environment (ISME). She is currently an Assistant Professor with the Department of Engineering for Innovation, University of Salento. She has published over 20 papers in the field and has contributed to several national and international projects in the area of robotics and autonomous underwater vehicles. Her research interests include modeling, navigation, guidance, and control of autonomous robotic vehicles, marine robotics, observers and estimation theory, modeling and parameter identification, and outlier robust filtering. She serves as an Associate Editor for *Control Engineering Practice*.

SIMONE DE NICOLI was born in Gallipoli, Italy, in 1997. He received the M.Sc. degree (Hons.) in computer engineering from the University of Salento, Lecce, Italy, in 2023. Since 2023, he has been a Computer Consultant and deals with the maintenance of e-commerce platforms. He is passionate about technology and the open-source world.

GIANFRANCO PARLANGELI (Member, IEEE) received the M.Sc. degree (Hons.) in electrical engineering from the University of Pisa, Pisa, Italy, in 1999, and the Ph.D. degree in information engineering from the University of Lecce, Lecce, Italy, in 2005. He is currently an Associate Professor with the Department of Engineering for Innovation, University of Salento, Lecce. He has published over 60 articles in the field and has contributed to several national and international projects in the areas of robotics and industrial automation. His research interests include analysis and design of multi-agent systems and robotic networks, fault tolerant control, variable structure control systems, and robotics. He is a member of the Scientific Committee of the Interuniversity Center of Integrated Systems for the Marine Environment (ISME).

Open Access funding provided by 'Università del Salento' within the CRUI CARE Agreement